Figure 6. *Stra8-Cre* expression delineates distinct spermatogonial populations.

A Representative flow cytometric analysis of GFP and c-Kit expression by the Plzf-positive testis cell population from 2 weeks postnatal *Z/EG; Stra8-Cre* mice. Quadrant gates were set according to wild-type control mice. The fraction of cells within quadrant gates is indicated.

B Representative FSC plot overlay of the indicated testis cell fractions from 2 weeks postnatal *Z/EG; Stra8-Cre* mice as in (A) (left panel; Ctrl). FSC plots of the equivalent populations from rapamycin-treated *Z/EG; Stra8-Cre* mice are shown (right panel; Rapa).

C Quantification of the flow cytometry analysis shown in (B). Graph shows mean FSC values of the indicated testis cell fractions from *Z/EG; Stra8-Cre* mice. Horizontal bars represent mean values; three mice were analyzed. $*P < 0.05$; $**P < 0.01$.

D Representative whole-mount images of *Z/EG; Stra8-Cre* juvenile (upper panels) and adult (lower panels) seminiferous tubules illustrating positive association between GFP expression and phospho-4EBP1 staining within the Plzf-positive population. Dashed outlines indicate Plzf-positive cysts of varying lengths. A_{al} are generally positive for both GFP and P-4EBP, while GFP-negative Plzf-positive cells are often A_s and A_{pr} and P-4EBP negative/low. Arrowheads indicate occasional Plzf-positive cells that are P-4EBP positive but GFP negative. Duplicate samples from independent animals at both ages were analyzed.

E Representative whole-mount images of *Z/EG; Stra8-Cre* seminiferous tubules from juvenile mice assessing GFP expression in Gfrα1-positive (upper panels) and RARγ-positive (lower panels) spermatogonial populations. Arrowheads indicate Gfrα1-positive GFP-negative cells.

F Quantification of whole-mount analysis from (E). Graph indicates percentage of cells within the indicated spermatogonial populations negative for GFP. Mean values are shown from three independent juvenile mice ± SEM. A total of 12–15 mm of tubule length was analyzed per sample. $**P < 0.01$.

G FSC plot overlay of $Plzf^{pos}$ c-Kit^{neg} SPC testis cell fractions from 2 weeks postnatal wild-type mice divided according to RARγ expression. Testis cells were pooled from 2 littermate mice for analysis. Plot is representative from two independent experiments.

H Model depicting subdivision of SPCs according to mTORC1 activity status. These subpopulations have distinct self-renewal capabilities (curved arrows) and differentiation tendencies. Levels of mTORC1 activity in the different cell fractions are indicated, and the predicted hierarchy between the populations under steady-state conditions is shown. Markers associated with the distinct populations are indicated, as is the expression pattern of the *Stra8-Cre* transgene. Dashed arrow represents proposed capability of differentiation-prone SPC subsets to contribute to self-renewing pool during regeneration. Balanced self-renewal and differentiation of the SPC pool is dependent on the TSC1/2 complex, which inhibits adoption of an mTORC1-active, differentiation-prone state.

Data information: Scale bars are 50 μm. Dotted lines in whole mounts indicate the seminiferous tubule profile.

activation of this signaling complex defines the distinct functional characteristics of these SPC subsets (Fig 6H). Therefore, in response to *Vasa-Cre*-driven *Tsc2* deletion, the mTORC1-low self-renewing subsets would be converted into an mTORC1-active state characterized by a high propensity for differentiation. This would cause a switch in the overall balance of cell fate from self-renewal to differentiation and ultimately lead to SPC exhaustion and germline degeneration.

Our study demonstrates that the TSC complex is an important cell-intrinsic regulator of the mTORC1 signaling pathway in SPCs and would act to control the equilibrium between mTORC1-low and mTORC1-active populations (Fig 6H). However, whether the observed disparity in mTORC1 activation by SPC subsets is due to intrinsic mechanisms or extrinsic cues is not clear. Growth factors are major cell-extrinsic regulatory inputs of the mTORC1 pathway, of which a variety have described expression in the testis and can activate mTORC1 through upstream PI3Kinase-Akt and Erk MAPK pathways [5,6,43]. Indeed, SPC maintenance and function is dependent on appropriate regulation of the PI3Kinase-Akt pathway [44]. Physical constraints of the SPC niche coupled with the localized production of growth factors by cells within the niche may underlie the observed differential mTORC1 activation within the SPC pool [45]. Notably, however, we find that mTORC1 activation within cells of the SPC niche (Sertoli cells) does not affect expression of key niche growth factors or appear to affect stem cell function, in contrast to other systems [33,34]. Further, local variations in the concentration of retinoic acid (RA), an important regulator of germ cell differentiation [46], may result in differential mTORC1 activation in SPCs; RA-dependent activation of mTORC1 is directly associated with differentiation in other cell systems [47]. Interestingly, *Stra8* was originally identified as an RA-responsive gene and RA-response elements are present within the proximal *Stra8* promoter used in the *Stra8-Cre* transgene [27,48,49]. Given that we find *Stra8-Cre* to be preferentially active within mTORC1-active SPC subsets, RA may represent an important extrinsic factor driving mTORC1 activation in SPCs. However, whether the mTORC1 pathway is a critical downstream target for RA-dependent induction of SPC differentiation remains to be determined.

Conserved function of the mTORC1 pathway in adult stem cell regulation

A role for mTORC1 in SPC maintenance was originally proposed from studies of the $Plzf^{-/-}$ mouse [6]. By conditional deletion of *Tsc2* in SPCs, we now confirm a key role for this signaling pathway in SPC fate decisions. Interestingly, disruption of either *Tsc1* or *Tsc2* genes in germline stem cells (GSCs) of the *Drosophila* ovary results in their differentiation and loss in an mTORC1-dependent manner [50,51], indicating a conserved role for the TSC complex in regulation of GSC fate. Increased activation of mTORC1 in SPCs/GSCs of both mouse and *Drosophila* inhibits response of the cells to key niche-derived signals required for self-renewal [6,51], providing a novel mechanism by which mTORC1 can control the functional properties of stem cells. Specifically, in SPCs, mTORC1 can inhibit expression of GDNF receptor components, thus preventing maintenance of the undifferentiated state [6,31,52]. Transcriptional profiling of SPCs upon mTORC1 inhibition *in vivo* has revealed numerous changes in expression of genes involved in the oxidative stress response, signal transduction pathways and SPC regulation [53]. Indeed, many cellular processes controlled by mTORC1, including mRNA translation, autophagy and metabolism [17], are implicated in stem cell regulation [14,54,55]. Thus, besides the GDNF receptor, multiple downstream targets of mTORC1 may be relevant in controlling SPC fate.

Intriguing parallels can also be drawn between the roles of mTORC1 in spermatogenesis and neurogenesis, since a direct association between mTORC1 activation and neural differentiation is evident from studies in multiple model systems. For example, neuronal progenitor differentiation in developing *Drosophila* is induced by mTORC1 acting downstream insulin receptor signaling [56]. In the mouse, *Tsc1* deletion and aberrant mTORC1 activation in embryonic neural stem cells (NSCs) triggers a reduction in

self-renewal capacity and premature differentiation [16]. Remarkably, negative feedback between mTORC1 and the upstream PI3Kinase-Akt pathway was proposed to underlie this reduction in NSC self-renewal [16], similar to the effects of chronic mTORC1 activation on GDNF-dependent Akt activation in SPCs from the *Plzf*$^{-/-}$ model [6]. Interestingly, in rodent models of neuroprogenitor differentiation, mTORC1 pathway inhibition through *Redd1* induction is reported to oppose differentiation onset [57]. Importantly, in this latter study, differentiation stimuli transiently induce *Redd1*, thus limiting mTORC1 activation and reducing progenitor depletion through differentiation. It can be significant that we find *Redd1* to be regulated in an mTORC1-dependent fashion at both mRNA and protein levels in cultured SPCs (Supplementary Fig S6) [6]. Thus, in response to mTORC1-activating stimuli, Redd1 can act as part of a negative feedback circuit to limit the fraction of SPCs that transition to an mTORC1-high state and which are ultimately likely to differentiate.

In summary, we characterize an unappreciated heterogeneity within the SPC pool based on differential mTORC1 activity and demonstrate the key instructive role played by the mTORC1 pathway in the regulation of SPC fate. Given that the mTORC1 pathway is regulated in a dynamic fashion, these studies also suggest a mechanistic basis for the differing yet reversible differentiation tendencies of discrete SPC subsets [7]. Further, as mTORC1 plays a seemingly conserved role in regulation of adult stem cell function, it will be interesting to assess whether activity of this pathway drives observed functional heterogeneity of stem cells in other tissues.

Materials and Methods

Mouse maintenance and treatments

Mice carrying floxed *Tsc2* alleles are previously described [58]. *Stra8-Cre*, *Vasa-Cre*, *Amh-Cre* and *Z/EG* reporter mice were obtained from Jackson Laboratories. The *Vasa-Cre* transgene was carried from males of breeding pairs due to maternal effects that result in whole-body Cre-mediated recombination in offspring [12,29]. When *Vasa-Cre* is carried from males, low-level *Cre* expression during zygotic development can result in global Cre-mediated recombination in offspring [29], resulting in embryonic lethality with *Tsc2* deletion. Expected frequency of obtaining *Tsc2*$^{F/\Delta}$ *Vasa-Cre* mice from mating *Tsc2*$^{F/+}$ *Vasa-Cre* males with *Tsc2*$^{F/F}$ females is 1:4, and observed frequency was ~1:20. Both *Stra8-Cre* and *Amh-Cre* transgenes were carried from females. Juvenile mice were routinely analyzed at 2 weeks of age. Mice were treated with rapamycin or vehicle daily for 7 days starting at postnatal day 10 as described [6]. All animal experiments were subject to approval by the Institutional Animal Care and Use Committee of Beth Israel Deaconess Medical Center and the Monash University Animal Ethics Committee.

Immunohistochemistry (IHC) and histology

Testis tissue was fixed in 4% paraformaldehyde (PFA) prior to embedding in paraffin and processing for IHC and histology as described [12]. Primary antibodies used were as follows: polyclonal anti-phospho RPS6 (Ser235/236) and polyclonal anti-LIN28A (Cell Signaling Technology), monoclonal anti-Plzf (clone 9E12) [6], rabbit monoclonal anti-TSC2, C-term (Epitomics) and polyclonal anti-Sox9 (Chemicon). Nuclei counterstains were performed with hematoxylin or DAPI.

Whole-mount immunofluorescence

Testes were detunicated and seminiferous tubules teased apart and rinsed in phosphate-buffered saline (PBS) on ice. Tubules were fixed with 4% PFA for 6 h at 4°C and washed in PBS prior to blocking in 0.3% PBS Triton X-100 (PBSX) supplemented with 5% fetal bovine serum (FBS) and 1% bovine serum albumin (BSA). Tubules were incubated overnight at 4°C with primary antibodies diluted in PBSX containing 1% BSA. Samples were washed in PBSX and primary antibodies detected with appropriate Alexa Fluor-conjugated secondary antibodies (Jackson ImmunoResearch). Tubules were mounted in Vectashield mounting medium (Vector Labs) and analyzed with an Axio Imager Z1 m with Apotome (Zeiss) or Nikon Invert C1 confocal microscope at the Monash University Micro Imaging facility. Primary antibodies used were as follows: goat anti-PLZF, anti-Gfrα1 and anti-Lin28a (R&D Systems), chicken anti-GFP (Abcam), monoclonal rabbit anti-phospho RPS6 (Ser235/236), anti-phospho 4E-BP1 (Thr37/46), anti-non-phospho 4E-BP1 (Thr46), anti-Lin28a and anti-RARγ1 (Cell Signaling Technology).

Flow cytometry

Methodology for intracellular staining and flow cytometric analysis of testis cells has been detailed previously [12]. Briefly, single cell suspensions obtained from the sequential digestion of testes with collagenase and trypsin were fixed in Cytofix buffer and permeabilized in Phosflow Perm buffer III (BD Biosciences) prior to immunostaining. Primary antibodies were as follows: Alexa 488- or Alexa 647-conjugated anti-Plzf [12], phycoerythrin (PE)-conjugated anti-c-Kit/CD117 (eBioscience), rabbit monoclonal anti-TSC2 and anti-mTOR (Epitomics), rabbit or chicken polyclonal anti-GFP (Invitrogen and Abcam) and monoclonal rabbit anti-4EBP1 and RARγ1 (Cell Signaling Technology). Primary antibodies were detected as appropriate with Alexa 488- and 647-conjugated secondary antibodies (Invitrogen and Jackson ImmunoResearch). Samples were run on an LSRII (BD Biosciences) and data were analyzed with FlowJo software (Tree Star).

qRT–PCR

RNA was extracted from testes and cultured SPCs using TRIzol reagent (Invitrogen) and treated with DNase prior to cDNA synthesis with a first-strand synthesis kit (Affymetrix). Cultured SPCs were washed off embryonic fibroblast feeder cells prior to RNA extraction [6]. Quantitative PCRs were run on a LightCycler (Roche) using a QuantiTect SYBR Green PCR kit (Qiagen). Primer sequences were previously described [6,36].

Statistical analysis

Assessment of statistical significance was performed using a 2-tailed *t*-test. *P*-values are indicated as follows: $*P < 0.05$; $**P < 0.01$; $***P < 0.001$; not significant (ns) $P > 0.05$.

Supplementary information for this article is available online: http://embor.embopress.org

Acknowledgements
We would like to thank all members of the Pandolfi and Hobbs laboratories for helpful discussion. We are especially grateful for the experimental assistance and advice of Ai-Leen Chan, Mia De Seram and Antonella Papa. This work was supported by NIH grants to PPP and NHMRC Project Grant APP1062197 to RMH. JM is supported by a fellowship from the Sigrid Jusélius Foundation.

Author contributions
RMH and PPP conceived and designed the study. RMH, HML and JM performed the experiments and data analysis. RMH, HML and PPP wrote the paper. TK and TN provided critical reagents.

Conflict of interest
The authors declare that they have no conflict of interests.

References

1. De Rosa L, De Luca M (2012) Cell biology: dormant and restless skin stem cells. *Nature* 489: 215 – 217
2. Carlone DL, Breault DT (2012) Tales from the crypt: the expanding role of slow cycling intestinal stem cells. *Cell Stem Cell* 10: 2 – 4
3. Mascre G, Dekoninck S, Drogat B, Youssef KK, Brohee S, Sotiropoulou PA, Simons BD, Blanpain C (2012) Distinct contribution of stem and progenitor cells to epidermal maintenance. *Nature* 489: 257 – 262
4. Fuchs E (2009) The tortoise and the hair: slow-cycling cells in the stem cell race. *Cell* 137: 811 – 819
5. Oatley JM, Brinster RL (2012) The germline stem cell niche unit in mammalian testes. *Physiol Rev* 92: 577 – 595
6. Hobbs RM, Seandel M, Falciatori I, Rafii S, Pandolfi PP (2010) Plzf regulates germline progenitor self-renewal by opposing mTORC1. *Cell* 142: 468 – 479
7. Nakagawa T, Sharma M, Nabeshima Y, Braun RE, Yoshida S (2010) Functional hierarchy and reversibility within the murine spermatogenic stem cell compartment. *Science* 328: 62 – 67
8. Hara K, Nakagawa T, Enomoto H, Suzuki M, Yamamoto M, Simons BD, Yoshida S (2014) Mouse spermatogenic stem cells continually interconvert between equipotent singly isolated and syncytial states. *Cell Stem Cell* 14: 658 – 672
9. Nakagawa T, Nabeshima Y, Yoshida S (2007) Functional identification of the actual and potential stem cell compartments in mouse spermatogenesis. *Dev Cell* 12: 195 – 206
10. Buaas FW, Kirsh AL, Sharma M, McLean DJ, Morris JL, Griswold MD, de Rooij DG, Braun RE (2004) Plzf is required in adult male germ cells for stem cell self-renewal. *Nat Genet* 36: 647 – 652
11. Costoya JA, Hobbs RM, Barna M, Cattoretti G, Manova K, Sukhwani M, Orwig KE, Wolgemuth DJ, Pandolfi PP (2004) Essential role of Plzf in maintenance of spermatogonial stem cells. *Nat Genet* 36: 653 – 659
12. Hobbs RM, Fagoonee S, Papa A, Webster K, Altruda F, Nishinakamura R, Chai L, Pandolfi PP (2012) Functional Antagonism between Sall4 and Plzf Defines Germline Progenitors. *Cell Stem Cell* 10: 284 – 298
13. Castilho RM, Squarize CH, Chodosh LA, Williams BO, Gutkind JS (2009) mTOR mediates Wnt-induced epidermal stem cell exhaustion and aging. *Cell Stem Cell* 5: 279 – 289
14. Chen C, Liu Y, Liu R, Ikenoue T, Guan KL, Zheng P (2008) TSC-mTOR maintains quiescence and function of hematopoietic stem cells by repressing mitochondrial biogenesis and reactive oxygen species. *J Exp Med* 205: 2397 – 2408
15. Ito K, Bernardi R, Pandolfi PP (2009) A novel signaling network as a critical rheostat for the biology and maintenance of the normal stem cell and the cancer-initiating cell. *Curr Opin Genet Dev* 19: 51 – 59
16. Magri L, Cambiaghi M, Cominelli M, Alfaro-Cervello C, Cursi M, Pala M, Bulfone A, Garcìa-Verdugo JM, Leocani L, Minicucci F *et al* (2011) Sustained activation of mTOR pathway in embryonic neural stem cells leads to development of tuberous sclerosis complex-associated lesions. *Cell Stem Cell* 9: 447 – 462
17. Laplante M, Sabatini DM (2012) mTOR signaling in growth control and disease. *Cell* 149: 274 – 293
18. Hsieh AC, Liu Y, Edlind MP, Ingolia NT, Janes MR, Sher A, Shi EY, Stumpf CR, Christensen C, Bonham MJ *et al* (2012) The translational landscape of mTOR signalling steers cancer initiation and metastasis. *Nature* 485: 55 – 61
19. Thoreen CC, Chantranupong L, Keys HR, Wang T, Gray NS, Sabatini DM (2012) A unifying model for mTORC1-mediated regulation of mRNA translation. *Nature* 485: 109 – 113
20. Düvel K, Yecies JL, Menon S, Raman P, Lipovsky AI, Souza AL, Triantafellow E, Ma Q, Gorski R, Cleaver S *et al* (2010) Activation of a metabolic gene regulatory network downstream of mTOR complex 1. *Mol Cell* 39: 171 – 183
21. Ahmed EA, de Rooij DG (2009) Staging of mouse seminiferous tubule cross-sections. *Methods Mol Biol* 558: 263 – 277
22. Ma XM, Blenis J (2009) Molecular mechanisms of mTOR-mediated translational control. *Nat Rev Mol Cell Biol* 10: 307 – 318
23. Kang SA, Pacold ME, Cervantes CL, Lim D, Lou HJ, Ottina K, Gray NS, Turk BE, Yaffe MB, Sabatini DM (2013) mTORC1 phosphorylation sites encode their sensitivity to starvation and rapamycin. *Science* 341: 1236566
24. Chakraborty P, Buaas FW, Sharma M, Snyder E, de Rooij DG, Braun RE (2014) LIN28A marks the spermatogonial progenitor population and regulates its cyclic expansion. *Stem Cells* 32: 860 – 873
25. Kobayashi T, Minowa O, Sugitani Y, Takai S, Mitani H, Kobayashi E, Noda T, Hino O (2001) A germ-line Tsc1 mutation causes tumor development and embryonic lethality that are similar, but not identical to, those caused by Tsc2 mutation in mice. *Proc Natl Acad Sci USA* 98: 8762 – 8767
26. Onda H, Lueck A, Marks PW, Warren HB, Kwiatkowski DJ (1999) Tsc2(±) mice develop tumors in multiple sites that express gelsolin and are influenced by genetic background. *J Clin Invest* 104: 687 – 695
27. Sadate-Ngatchou PI, Payne CJ, Dearth AT, Braun RE (2008) Cre recombinase activity specific to postnatal, premeiotic male germ cells in transgenic mice. *Genesis* 46: 738 – 742
28. Fingar DC, Salama S, Tsou C, Harlow E, Blenis J (2002) Mammalian cell size is controlled by mTOR and its downstream targets S6K1 and 4EBP1/eIF4E. *Genes Dev* 16: 1472 – 1487
29. Gallardo T, Shirley L, John GB, Castrillon DH (2007) Generation of a germ cell-specific mouse transgenic Cre line, Vasa-Cre. *Genesis* 45: 413 – 417
30. Zheng K, Wu X, Kaestner KH, Wang PJ (2009) The pluripotency factor LIN28 marks undifferentiated spermatogonia in mouse. *BMC Dev Biol* 9: 38
31. Naughton CK, Jain S, Strickland AM, Gupta A, Milbrandt J (2006) Glial cell-line derived neurotrophic factor-mediated RET signaling regulates spermatogonial stem cell fate. *Biol Reprod* 74: 314 – 321
32. Meng X, Lindahl M, Hyvönen ME, Parvinen M, de Rooij DG, Hess MW, Raatikainen-Ahokas A, Sainio K, Rauvala H, Lakso M *et al* (2000)

Regulation of cell fate decision of undifferentiated spermatogonia by GDNF. *Science* 287: 1489 – 1493

33. Kobayashi H, Butler JM, O'Donnell R, Kobayashi M, Ding BS, Bonner B, Chiu VK, Nolan DJ, Shido K, Benjamin L *et al* (2010) Angiocrine factors from Akt-activated endothelial cells balance self-renewal and differentiation of haematopoietic stem cells. *Nat Cell Biol* 12: 1046 – 1056
34. Yilmaz ÖH, Katajisto P, Lamming DW, Gültekin Y, Bauer-Rowe KE, Sengupta S, Birsoy K, Dursun A, Yilmaz VO, Selig M *et al* (2012) mTORC1 in the Paneth cell niche couples intestinal stem-cell function to calorie intake. *Nature* 486: 490 – 495
35. Holdcraft RW, Braun RE (2004) Androgen receptor function is required in Sertoli cells for the terminal differentiation of haploid spermatids. *Development* 131: 459 – 467
36. Payne CJ, Gallagher SJ, Foreman O, Dannenberg JH, Depinho RA, Braun RE (2010) Sin3a is required by sertoli cells to establish a niche for undifferentiated spermatogonia, germ cell tumors, and spermatid elongation. *Stem Cells* 28: 1424 – 1434
37. Tanwar PS, Kaneko-Tarui T, Zhang L, Teixeira JM (2012) Altered LKB1/AMPK/TSC1/TSC2/mTOR signaling causes disruption of Sertoli cell polarity and spermatogenesis. *Hum Mol Genet* 21: 4394 – 4405
38. Tanwar PS, Kaneko-Tarui T, Zhang L, Rani P, Taketo MM, Teixeira J (2010) Constitutive WNT/beta-catenin signaling in murine Sertoli cells disrupts their differentiation and ability to support spermatogenesis. *Biol Reprod* 82: 422 – 432
39. Munsterberg A, Lovell-Badge R (1991) Expression of the mouse anti-mullerian hormone gene suggests a role in both male and female sexual differentiation. *Development* 113: 613 – 624
40. Anderson EL, Baltus AE, Roepers-Gajadien HL, Hassold TJ, de Rooij DG, van Pelt AM, Page DC (2008) Stra8 and its inducer, retinoic acid, regulate meiotic initiation in both spermatogenesis and oogenesis in mice. *Proc Natl Acad Sci USA* 105: 14976 – 14980
41. Novak A, Guo C, Yang W, Nagy A, Lobe CG (2000) Z/EG, a double reporter mouse line that expresses enhanced green fluorescent protein upon Cre-mediated excision. *Genesis* 28: 147 – 155
42. Gely-Pernot A, Raverdeau M, Celebi C, Dennefeld C, Feret B, Klopfenstein M, Yoshida S, Ghyselinck NB, Mark M (2012) Spermatogonia differentiation requires retinoic acid receptor gamma. *Endocrinology* 153: 438 – 449
43. Ishii K, Kanatsu-Shinohara M, Toyokuni S, Shinohara T (2012) FGF2 mediates mouse spermatogonial stem cell self-renewal via upregulation of Etv5 and Bcl6b through MAP2K1 activation. *Development* 139: 1734 – 1743
44. Goertz MJ, Wu Z, Gallardo TD, Hamra FK, Castrillon DH (2011) Foxo1 is required in mouse spermatogonial stem cells for their maintenance and the initiation of spermatogenesis. *J Clin Invest* 121: 3456 – 3466
45. Yoshida S, Sukeno M, Nabeshima Y (2007) A vasculature-associated niche for undifferentiated spermatogonia in the mouse testis. *Science* 317: 1722 – 1726
46. Sugimoto R, Nabeshima Y, Yoshida S (2012) Retinoic acid metabolism links the periodical differentiation of germ cells with the cycle of Sertoli cells in mouse seminiferous epithelium. *Mech Dev* 128: 610 – 624
47. Carnevalli LS, Masuda K, Frigerio F, Le Bacquer O, Um SH, Gandin V, Topisirovic I, Sonenberg N, Thomas G, Kozma SC (2010) S6K1 plays a critical role in early adipocyte differentiation. *Dev Cell* 18: 763 – 774
48. Giuili G, Tomljenovic A, Labrecque N, Oulad-Abdelghani M, Rassoulzadegan M, Cuzin F (2002) Murine spermatogonial stem cells: targeted transgene expression and purification in an active state. *EMBO Rep* 3: 753 – 759
49. Oulad-Abdelghani M, Bouillet P, Decimo D, Gansmuller A, Heyberger S, Dolle P, Bronner S, Lutz Y, Chambon P (1996) Characterization of a premeiotic germ cell-specific cytoplasmic protein encoded by Stra8, a novel retinoic acid-responsive gene. *J Cell Biol* 135: 469 – 477
50. LaFever L, Feoktistov A, Hsu HJ, Drummond-Barbosa D (2010) Specific roles of Target of rapamycin in the control of stem cells and their progeny in the Drosophila ovary. *Development* 137: 2117 – 2126
51. Sun P, Quan Z, Zhang B, Wu T, Xi R (2010) TSC1/2 tumour suppressor complex maintains Drosophila germline stem cells by preventing differentiation. *Development* 137: 2461 – 2469
52. Jijiwa M, Kawai K, Fukihara J, Nakamura A, Hasegawa M, Suzuki C, Sato T, Enomoto A, Asai N, Murakumo Y, Takahashi M (2008) GDNF-mediated signaling via RET tyrosine 1062 is essential for maintenance of spermatogonial stem cells. *Genes Cells* 13: 365 – 374
53. Kofman AE, McGraw MR, Payne CJ (2012) Rapamycin increases oxidative stress response gene expression in adult stem cells. *Aging (Albany NY)* 4: 279 – 289
54. Suda T, Takubo K, Semenza GL (2011) Metabolic regulation of hematopoietic stem cells in the hypoxic niche. *Cell Stem Cell* 9: 298 – 310
55. Sampath P, Pritchard DK, Pabon L, Reinecke H, Schwartz SM, Morris DR, Murry CE (2008) A hierarchical network controls protein translation during murine embryonic stem cell self-renewal and differentiation. *Cell Stem Cell* 2: 448 – 460
56. Bateman JM, McNeill H (2004) Temporal control of differentiation by the insulin receptor/tor pathway in Drosophila. *Cell* 119: 87 – 96
57. Malagelada C, Lopez-Toledano MA, Willett RT, Jin ZH, Shelanski ML, Greene LA (2011) RTP801/REDD1 regulates the timing of cortical neurogenesis and neuron migration. *J Neurosci* 31: 3186 – 3196
58. Shigeyama Y, Kobayashi T, Kido Y, Hashimoto N, Asahara S-i, Matsuda T, Takeda A, Inoue T, Shibutani Y, Koyanagi M *et al* (2008) Biphasic response of pancreatic beta-cell mass to ablation of tuberous sclerosis complex 2 in mice. *Mol Cell Biol* 28: 2971 – 2979

SCIENTIFIC REPORTS

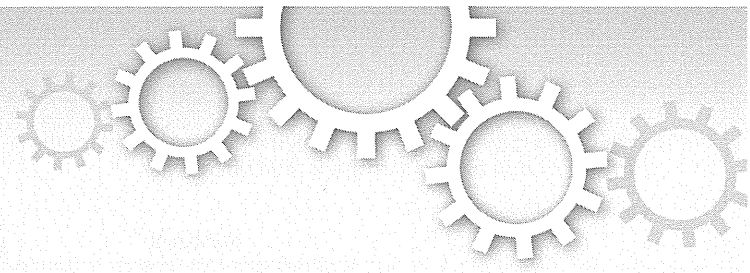

OPEN

SUBJECT AREAS:
CANCER MODELS
TUMOUR SUPPRESSORS

Received
7 April 2014

Accepted
19 June 2014

Published
4 August 2014

Correspondence and requests for materials should be addressed to O.H. (ohino@med.juntendo.ac.jp)

Transgenic expression of the N525S-tuberin variant in *Tsc2* mutant (Eker) rats causes dominant embryonic lethality

Masatoshi Shiono[1,2], Toshiyuki Kobayashi[2], Riichi Takahashi[3,4], Masatsugu Ueda[3,5], Chikashi Ishioka[1,6] & Okio Hino[2]

[1]Department of Clinical Oncology, Tohoku University Hospital, Tohoku University, 1-1 Seiryo-machi, Aoba-ku, Sendai, Miyagi 980-8574, Japan, [2]Department of Pathology and Oncology, Juntendo University School of Medicine, 2-1-1 Hongo, Bunkyo-ku, Tokyo 113-8421, Japan, [3]PhoenixBio Co., Ltd., 1198-4 Iwazo-machi, Utsunomiya, Tochigi 321-0973, Japan, [4]Animal Resources Center, Central Institute for Experimental Animals, 3-25-12 Tonomachi, Kawasaki, Kangawa 210-0821, Japan, [5]Transgenic Animal Division, Utsunomiya Institute, Institute of Immunology Co., Ltd., 1198-4 Iwazo-machi, Utsunomiya, Tochigi 321-0973, Japan, [6]Department of Clinical Oncology, Institute of Development, Aging, and Cancer, Tohoku University, 4-1 Seiryo-machi, Aoba-ku, Sendai, Miyagi 980-8575, Japan.

The *Tsc2* product, tuberin, negatively regulates the mTOR pathway. We have exploited the Eker (*Tsc2*-mutant) rat system to analyse various *Tsc2* mutations. Here, we focus on the N525S-*Tsc2* variant (NSM), which is known to cause distinct symptoms in patients even though normal suppression of mTOR is observed. Unexpectedly, we were repeatedly unable to generate viable rats carrying the NSM transgene. Genotypic analysis revealed that most of the embryos carrying the transgene died around embryonic day after 14.5—similar to the stage of lethality observed for Eker homozygotes. Thus, the NSM transgene appeared to have a dominant lethal effect in our rat model. Further, no significant differences were observed for various signal transduction molecules in transiently expressed NSM cells compared to WT. These results indicate that a non-mTOR pathway, critical for embryogenesis, is being regulated by tuberin, providing a link between tuberin expression and the severity of *Tsc2* mutation-related pathogenesis.

Tuberous sclerosis (TSC) is an inherited autosomal dominant disease characterised by skin lesions (hamartomas), central nervous system disorders (e.g., cerebral tubera, seizures, and mental retardation), and systemic multiple tumoral lesions (e.g. subependymal giant cell astrocytoma of brain, angiomyolipoma of kidney and liver, rhabdomyoma of heart, lymphangioleiomyomatosis of lung, retinal hamartoma, and angiofibroma) with an estimated prevalence of 1/6000[1]. The two tumour suppressor genes responsible for TSC, *TSC1* (9q34), and *TSC2* (16p13.3) have been identified and positionally cloned[2,3]. It is known that the protein products of *TSC1* (hamartin) and *TSC2* (tuberin) form a complex that exhibits GTPase-activating protein (GAP) function, converting Rheb, a small G protein located upstream of mTOR, into its inactive state[4,5]. This function results in the downregulation of the mTOR-S6K1 pathway (mTOR-axis)[6,7].

Further, analysis of familial TSC patients has indicated that the clinical symptoms may be dependent on the particular mutations/variations of tuberin[8–11]. Numerous mutations/variations exist in the *TSC2* gene, many of which have been reported to cause unusual mild symptoms[12,13]. Here, we have focused on two missense mutations that seemed to be correlated to the severity of symptoms and mTOR-axis regulation. Although the human G1556S mutation (GSM) in tuberin is located within the GAP-related domain and affects Rheb-GAP activity, patients carrying this mutation display mild symptoms, such as normal brain imaging, skin lesions, and only the occasional hamartoma on other tissues[14,15]. In contrast, the human N525S variant (NSM) in tuberin retains its Rheb-GAP activity, but the clinical manifestation of this variation is much more distinct, including cortical tubers, subependymal giant cell astrocytomas, renal angiomyolipomas, and cardiac rhabdomyomas[8,14,16,17]. Thus, the status of the mTOR-axis does not correlate with symptom severity in patients with these mutations, suggesting that the aberrant activation of the mTOR-axis, although it may play a major role, is not the sole determinant of TSC pathogenesis. Additional studies on GSM, NSM, and other tuberin variants, with emphasis

Table 1 | Generation of transgenic founder rats

Summary of injection

Gene	Number of Injected eggs	Transferred eggs	Born offspring	Tg(+) rats
pMGTsc2-GSM (G1556S-type)	135	127	53	5 | 4(Tsc2+/+) 1(Tsc2+/−)
pMGTsc2-NSM (N525S-type)	236	214	73	0
pMGTsc2-WT (Wild-type)	172	106	21	5 | 1(Tsc2+/+) 4(Tsc2+/−)

*Donor animals: Eker(Tsc2+/−) ♂ x Wistar(Tsc2+/+).
†Phenotype of rats carrying GSM- or WT-Tg were previously reported[23].

on the *in vivo* mechanisms of action, are necessary in order to identify the novel pathways involved in the development of TSC as well as new therapeutic targets.

Importantly, a homolog of human *TSC2* (*Tsc2*) in the Eker rat, first shown to develop hereditary renal cancer naturally in 1953[18], appears to be the gene responsible for this phenotype, making this animal model ideal for studying *Tsc2* function[19–21]. Rats heterozygous for *Tsc2* develop renal tumours by one year of age without exception and homozygotes are embryonic lethal. In a previous study, we generated transgenic Eker rats carrying the cDNA and promoter of wild-type rat *Tsc2*, and demonstrated that the transgene (Tg) inhibited both renal carcinogenesis in Eker heterozygotes and embryonic lethality in homozygotes[22]. Further, Eker rats carrying the GSM-tuberin variant also had suppressed tumour formation, even though the mTOR pathway was disrupted[23]. These data are consistent with the observation that patients carrying the GSM develop mild symptoms, suggesting that there is another pathway that regulates tumour progression, independent of the mTOR pathway. Correspondingly, we hypothesise that transgenic Eker rats carrying the NSM might develop severe tumorigenic phenotypes, albeit while retaining normal mTOR function, and thus, could provide a clue to uncover the novel function of Tsc2 related to tumour progression. To investigate this possibility, we have exploited the transgenic Eker rat system to express the NSM and subsequently characterised tuberin function and pathogenesis *in vivo*. In this analysis, both the wild-type- (WT-) and NSM-tuberin showed no difference in complex formation with hamartin, subcellular localisation, phosphorylation status, or mTOR inhibition *in vitro*. However, much to our surprise, we were unable to repeatedly generate viable newborn rats carrying the NSM Tg. In this study, we report an unexpected dominant effect of NSM-tuberin on development and cell growth.

Results

Our previous *in vitro* analyses showed that GSM-tuberin exhibited a change in the subcellular localisation (scattered throughout the cytosol), a weak interaction with hamartin, an altered phosphorylation status, and did not stimulate Rheb-GTPase activity or inhibit S6K and S6 phosphorylation[15,16,23]. In contrast, NSM-tuberin had characteristics similar to the WT-tuberin with regard to subcellular localisation (forming the perinuclear dense bodies; PNDBs), complex formation with hamartin at the PNDBs, phosphorylation status, and Rheb-GTPase activity (intact) along with S6K and S6 phosphorylation[14,16,17,23].

To further investigate the function of these tuberin mutants *in vivo* using our transgenic Eker rat system[22–24], we constructed Tgs for the expression of GSM- or NSM-tuberin (GSM Tg or NSM Tg, respectively). Our characterisation of the WT and GSM Tg rats has been reported previously[23]. Despite repeated attempts, we were unable to generate viable newborn rats carrying the NSM Tg (Table 1). This

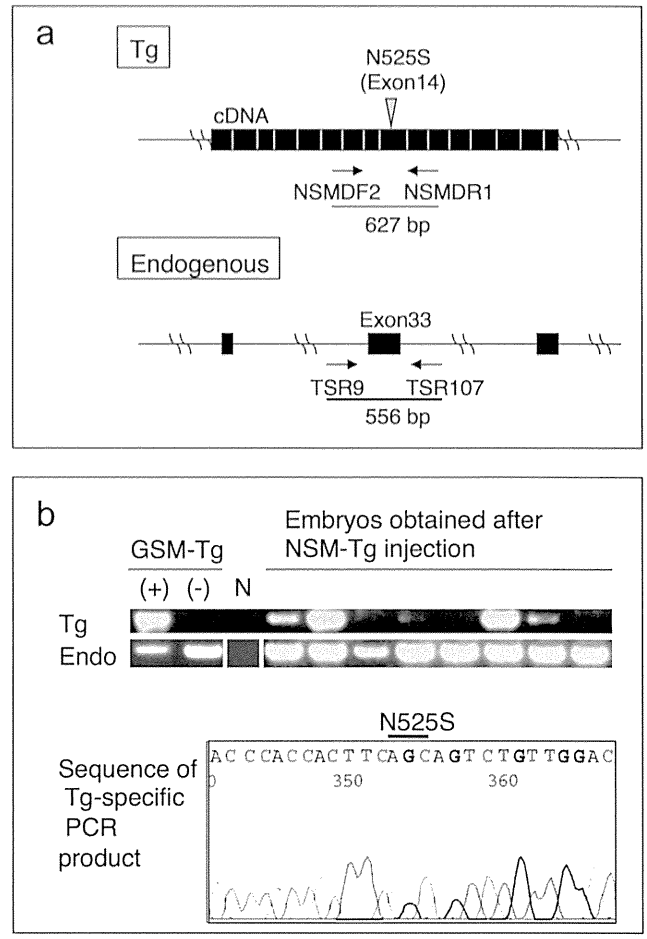

Figure 1 | Detection of NSM Tg-positive embryos. (a) Schematic diagram of the primers utilised for the Tg-specific and endogenous *Tsc2*-specific PCRs. Each filled box denotes the exon. (b) PCR genotyping results and sequencing analyses. Upper panel shows the PCR analysis of eight individual E10.5 embryos. DNAs from GSM Tg carrying (+) or non-carrying (−) rats were used as controls. Lane N indicates the template DNA negative control. Endogenous *Tsc2* was amplified as the PCR control (Endo). The blots have been cropped focusing on the bands or interest; See Supplementary Fig. S1 for full-length gels. Lower panel shows the sequence of the Tg-specific PCR product. The position of the N525S mutation is indicated.

result was unexpected as the *in vitro* characteristics of NSM-tuberin were similar to those of WT-tuberin[8,14,16,17]. We therefore screened embryos at different stages of gestation following injection of NSM Tg DNA. At embryonic day (E) 10.5, Tg-positive embryos were detected using Tg-specific PCR genotyping (Fig. 1a) and the inserted sequence was confirmed to be that of the NSM Tg (Fig. 1b). Then, we proceeded to determine the stage at which embryos carrying the NSM Tg die. The Eker homozygous condition is known to be lethal from day 13 to 18 of gestation[25,26]. Intriguingly, the frequency of live NSM Tg-positive embryos fell abruptly after the E14.5 stage, suggesting that many of the NSM Tg-positive embryos died during this stage[26] (Table 2). The similarity in the timing of embryonic lethality in homozygous $Tsc2^{Eker/Eker}$ mutants and NSM Tg carrying embryos might indicate that NSM-tuberin exerts a dominant negative effect on WT-tuberin function during embryonic rat development.

In order to further investigate the effects of NSM-tuberin, we tried to generate cell lines that stably expressed NSM *in vitro*. This type of methodology has been employed previously for WT-tuberin and, as NSM-tuberin exhibited similar characteristics to the WT construct

Table 2 | NSM Tg positive embyos

	Tg(+) embryos	Live embryos	Rate: Tg(+)/total
E10.5	11	22	0.500
E12.5	9	30	0.300
E14.5	6	22	0.273
E16.5	1	10	0.100
E18.5	2	16	0.125

in various transient expression experiments[23], expression was expected to result in similar phenotypic changes. Notably, since the aforementioned results indicated that stable expression of NSM-tuberin was predicted to exert some toxic cellular effects, we adopted a conditional gene expression system. However, despite our repeated attempts and changes to the tetracycline inducible expression system (RevTet-off System and Tet-On 3G System; Clontech, CA, USA) and the flow cytometry-based purification by tagged ZsGreen (with drug selection), none of these resulted in stable expression of NSM. In contrast, stable cell line expression of WT and GSM was successful (Fig. 2a–c). Therefore, we suspect that the NSM-tuberin has a dominant negative effect when it is constitutively expressed *in vivo* and *in vitro*.

To elucidate the mechanism of this putative dominant negative effect, we operated a series of additional *in vivo* (foetal tissue analysis) and *in vitro* (global analysis in major signal transduction pathways) analyses. In the tissue analysis, we observed no gross abnormalities or changes in individual embryo size at any stage irrespective of their NSM Tg genetic status (Fig. 3a). After examining sectioned embryonic NSM Tg positive tissues, exencephaly, which is frequently associated with lethality in Eker homozygotes and *Tsc1/2* knockout embryos[25–28], was not observed (Fig. 3b). In order to better understand this discrepancy in regards to the underlying mechanism, we performed a comprehensive analysis involving a variety of signal transduction molecules using transient expression cell lysates (Fig. 4a), whereby the relative tyrosine phosphorylation statuses of 44 different receptor tyrosine kinases (RTKs) were determined. Yet, no prominent difference was detected among the samples expressing control vector, WT-, or NSM-Tsc2 (Fig. 4b). In the Reverse Phase Protein Array (RPPA) analysis, 180 targets of the anti-phospho antibodies were also examined. However, the results among samples showed no distinct differences (Fig. 4c). Thus, no prominent difference was detected in any of the comprehensive analyses we adopted. Although further analyses are needed to elucidate the mechanism of these putative dominant negative effects, our data suggest the existence of a novel unknown pathway(s) that is, at least in part, regulated by NSM-tuberin *in vitro* and *in vivo*.

Discussion

mTOR is one of the major clinical therapeutic targets against cancer[29–31]. While mTOR inhibitors are prescribed to treat various tumours[32–36], mTOR itself also serves as a major target in T cell suppression for transplantation and autoimmune disease[37–39]. In a recent clinical trial, the oral mTOR inhibitor everolimus (rapamycin analogue) showed a marked 50% reduction in the subependymal giant cell astrocytoma (SEGA) volume in 32% of the TSC patients monitored[40]. Although this outcome is encouraging, this everolimus monotherapy was not effective in the other 68% of patients, suggesting that solely using an mTOR inhibitor is not sufficient to cure TSC. To address this issue, it is urgent that we investigate the existence of any unknown critical pathways, beyond the mTOR pathway, related to TSC pathogenesis in order to develop more successful therapeutic targets.

In many reports, NSM-tuberin showed similar characteristics to the WT-tuberin in various transient expression experiments[14,16,17]; however, the clinical manifestation of this variant in human patients is severe. Therefore, the possibility that TSC may, in some cases, develop independently of mTOR hyper-activation has been raised[17]. It is possible that other unknown functional defects in tuberin may be resulting in the severe disease phenotype, which may explain the unexpected embryonic lethality induced by the NSM Tg that we observed in this study in rats. Our analysis indicates that the majority of NSM Tg-carrying embryos died after E14.5, corresponding with the time period for the highest incidence of embryonic deaths in Eker homozygous mutant embryos[25,26]. Since we constructed the Tg using the intrinsic promoter of the wild-type *Tsc2*, it is possible that NSM expression is being induced in a spatiotemporally identical manner to endogenous *Tsc2* and the putative dominant negative effect against the endogenous *Tsc2* is occurring at the specific embryonic developmental stage when the gene begins to function. In regards to the similarity between the times of embryonic death for the two genotypes, we suggest that NSM affects normal embryonic development by generating a dominant negative effect in a pathway in which WT-tuberin has a function.

Furthermore, as there are human TSC patients with the N525S variation, we speculate that higher expression of the Tg compared to the endogenous gene may be required to exert the dominant-lethal effect when the wild-type *Tsc2* allele is present. Theoretically, in TSC patients with endogenous *TSC2* expression, the dominant negative function of N525S-tuberin could be elicited by inactivation of the wild-type *TSC2* allele and would be expected to induce severe symptoms. N525S has been suggested to be either a polymorphism[41] or a mutation[8,14,16,17]. Whichever is correct, it is certain that any type of variation in the *TSC* genes is likely playing a major role, potentially as a genetic modifier allele, in the susceptibility and phenotypic manifestation of the TSC-related disorders[42]. Hence, elucidation of the mechanism underlying the NSM-associated embryonic lethality at this stage of development will lead to the identification of a novel function of tuberin.

Here, we have demonstrated that NSM overexpression in rats causes embryonic lethality. Importantly, the N525S-type tuberin variant showed completely normal function when transiently expressed *in vitro* in regards to subcellular localisation, interaction with hamartin, phosphorylation, and mTOR regulation as compared to WT-tuberin. However, this variant also displayed a severe phenotype when stably expressed *in vitro* and *in vivo* (rats). To the best of our knowledge, this correlation between the function of tuberin and the severity of symptoms is completely novel and the elucidation of the unknown pathway through which NSM-tuberin functions will help to clarify the overall mechanism of TSC pathogenesis.

Methods

Plasmid construction. Schematic structures of the *Tsc2* transgene have been shown previously[23]. Generation of GSM and NSM rat *Tsc2* cDNAs and construction of the pCAG-FLAG-rTsc2-GSM and pCAG-FLAG-rTsc2-NSM plasmids were also reported previously[23]. NSM cDNA was used to replace the normal sequences in pMGTsc2-WT (the wild-type Tg used previously) in order to generate pMGTsc2-NSM. For the Tet-inducible systems, *Tsc2* cDNAs were cloned into pRev-TRE or pTRE3G-ZsGreen vectors (Clontech, CA, USA).

Microinjection and generation of transgenic founders. Wistar female rats (Purchased from Charles River Laboratories, Kanagawa, Japan) were injected intraperitoneally with hormone to stimulate ovulation and then mated with male Eker rats heterozygous for the *Tsc2* mutation. Fertilised eggs at the pronuclear stage were collected from impregnated females. Tg DNAs were linearised with *Not*I, purified using a QIAquick kit (QIAGEN, Hilden, Germany), and microinjected into the fertilised eggs[43]. The eggs were then transferred into the oviducts of pseudo-pregnant Wistar females.

Genotyping. DNA was prepared from adult tails or embryonic tissues (whole embryo, placenta, or yolk sac) by proteinase K digestion and phenol extraction. For Southern blot analysis, 10 μg of DNA was digested with *Bam*HI, subjected to 1% agarose gel electrophoresis, transferred onto a nylon membrane, and hybridised as described previously[21]. An *Eco*RI-*Bam*HI rat *Tsc2* cDNA fragment covering exons 26-33 (1.1 kb) was used as a probe after ^{32}P-labelling. Genotyping by PCR was performed using the following primers: for endogenous *Tsc2*, TSR9 (5′-GCTTGTGCCTTCT-AACAGTG-3′, forward, intron 32) and TSR107 (5′-GCAACTTGGGGTTTGTGC-

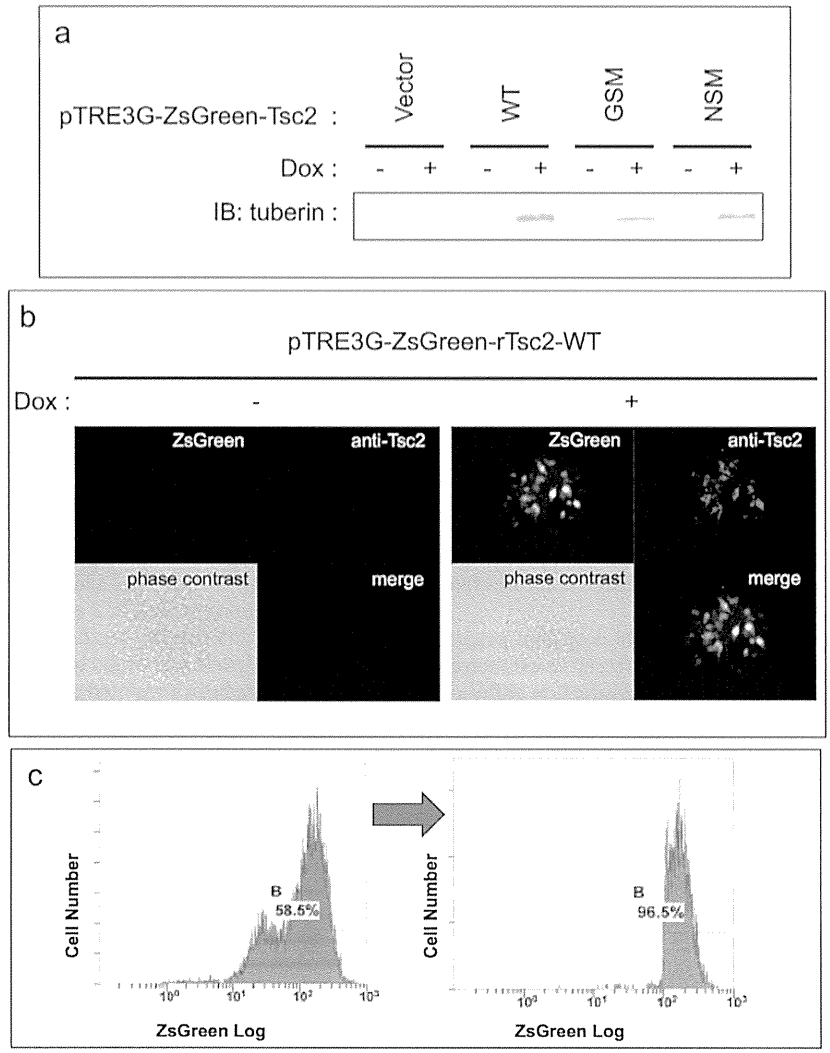

Figure 2 | Multiple attempts were made to establish cell lines stably expressing NSM-tuberin. (a) Tetracycline regulated the expression of each tuberin variant using Tet-on 3G system in HEK293 Tet-On 3G cells. Expression of each tuberin variant was appropriately induced by the presence or absence of doxycycline (Dox). Note that the previously reported band shift of GSM-tuberin compared to WT- or NSM-tuberin band was reproducible[15,23], suggesting that the system is working properly. The blots have been cropped, focusing on the bands or interest; See Supplementary Fig. S2 for full-length blots. (b) Tetracycline regulated the expression of each tuberin variant and ZsGreen using Tet-on 3G system in HEK293 Tet-On 3G cells. Representative immunofluorescent images are shown. Simultaneous tuberin variant and ZsGreen expression utilising IRES sequence was properly regulated by the presence or absence of Dox. (c) Representative flow cytometry (FCM) data showing the purification of ZsGreen-positive cells. The horizontal and vertical axes show the logarithmic fluorescent intensity and the number of cells, respectively. The percentages of the total live cells that were positive for ZsGreen are shown in each panel. Left panel; FCM before cell sorting (drug selection only). Although most cells are ZsGreen-positive, there are two peaks of cells in fluorescent intensity. To solve this heterogeneity in fluorescent intensity (indicating variable translational efficiency), cells were subjected to cell sorting. Right panel; FCM after cell sorting by gating stronger-ZsGreen-intensity peak. Subgroups of cells with weaker ZsGreen intensity (left peak in the left panel) were eliminated and subgroups with stronger ZsGreen intensity (right peak in the left panel) were purified by cell sorting. Cell lines stably expressing WT- and GSM-tuberin were successfully cultured, but despite numerous improvements in the methodology, cell lines that stably express NSM-tuberin were not obtained.

C-3′, reverse, intron 33); and for NSM, NSMDF2 (5′-AGTTCCACGGATCGCA-AGA-3′, forward, exon 11) and NSMDR1 (5′-TAGCAATGGGCAAGGAGTAG-3′, reverse, exon 16). The PCR amplification was performed using 35 cycles at 94°C for 1 min, 55°C for 1 min, and 72°C for 1.5 min.

Cell culture and transfection for transient expression. HEK293 cells were plated in collagen-coated 6-well plates at a density of 5×10^4 cells/well and cultured in Dulbecco's modified Eagle's medium supplemented with 10% foetal bovine serum (FBS) and penicillin/streptomycin. One day after plating, the HEK293 cells were transfected with plasmids (0.5 μg each) using FuGENE6 (Roche, Mannheim, Germany) according to the manufacturer's instructions. Cells were analysed after incubating 48 h.

Tetracycline (Tet) inducible expression system. The RevTet-off System or Tet-On 3G System were exploited to establish Tet-off or Tet-on cell lines, respectively, according to the manufacturer's instructions provided with the kits (Clontech, CA, USA). Briefly, HEK293 cells or HEK293 Tet-On 3G Cells (Clontech, CA, USA) were cultured in Dulbecco's modified Eagle's medium supplemented with 10% Tet System Approved FBS (Clontech, CA, USA) and recommended concentration of antibiotics for selection (e.g. G413, puromycin, hygromycin B) or gene expression (doxycycline) in appropriate steps. Cells were transfected using Xfect Transfection Reagent (Clontech, CA, USA) according to the manufacturer's instructions.

Antibodies. The following primary antibodies were used: anti-tuberin (C-20) from Santa Cruz Biotechnology (Santa Cruz, CA, USA); anti-FLAG and anti-beta-actin from Sigma (MO, USA); and anti-beta-tubulin III (clone TuJ1) from Babco (CA, USA).

Immunoblotting. Protein concentration was determined using the DC-protein assay (Bio-Rad, CA, USA). Cells were lysed with Laemmli buffer and equal amounts of

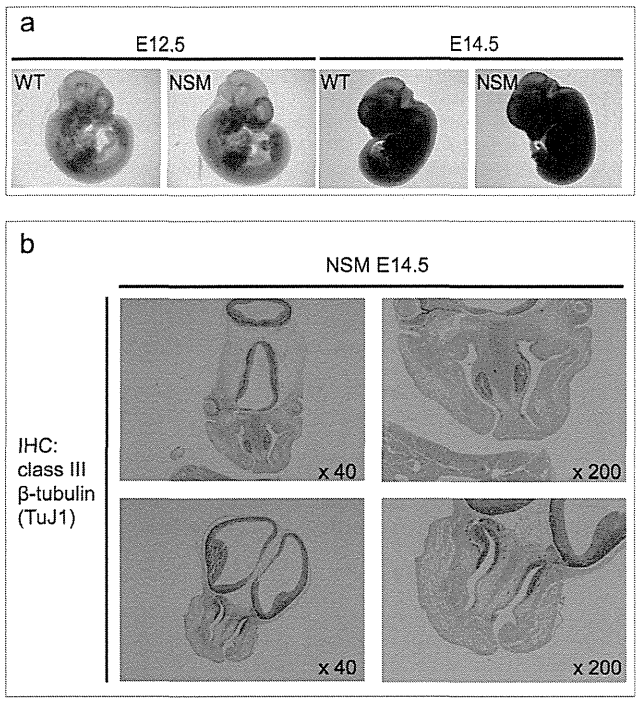

Figure 3 | Histological analysis of NSM Tg-positive embryos. (a) Macroscopic analysis of embryos. There were no apparent abnormalities or difference in size among individual embryos at any stage irrespective of their NSM Tg genetic status. (b) Class III beta-tubulin (TuJ1) immunohistochemical (IHC) analysis of embryonic tissue sections. Representative coronal sections of the embryo heads carrying NSM Tg are shown. Exencephaly, which is frequently associated with lethality in Eker homozygotes, was not observed.

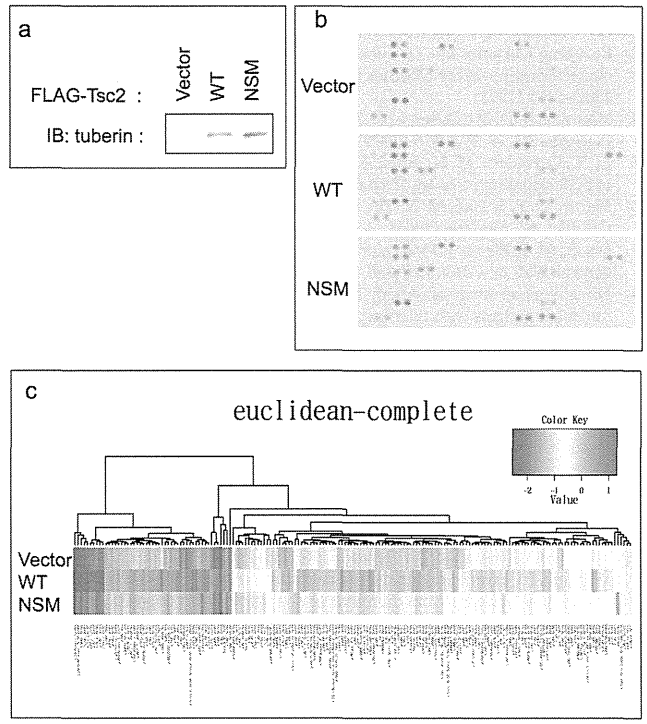

Figure 4 | Comprehensive analysis involving a variety of signal transduction molecules in transient expression of the tuberin variants. (a) Transient expression of the tuberin variants. HEK293 cells were transiently transfected with each expression vector plasmid and subjected to the following analyses. The blots have been cropped focusing on the bands or interest; See Supplementary Fig. S3 for full-length blots. (b) Phospho-Receptor Tyrosine Kinase (RTK) Array analysis. Levels of Phospho-RTK were assessed using a horseradish peroxidase-conjugated phospho-tyrosine antibody followed by chemiluminescence detection. No significant differences were observed in the relative tyrosine phosphorylation statuses of 44 different RTKs investigated in forced transient WT- or NSM-tuberin expressing cells. (c) Reverse Phase Protein Array (RPPA) analysis. The relative concentration values of the 180 anti-phospho antibody targets are represented as a heat map. No prominent differences were observed.

protein were separated by standard SDS-PAGE, followed by transfer onto a PVDF membrane (Millipore, MA, USA). Blocking was performed with Odyssey blocking buffer (Li-Cor Biosciences, Lincoln, NE, USA). The primary antibody was applied in the same blocking solution, followed by incubation with a goat anti-rabbit or a goat anti-mouse Alexa Fluor 680 secondary antibody (Invitrogen, Carlsbad, CA, USA). Antibody binding was detected and quantified using the Odyssey system (Li-Cor Biosciences).

Immunofluorescence. Cells were plated in a glass-bottomed dish (Matsunami, Osaka, Japan) at a density of 1×10^4 cells/well, transfected as described above, and fixed and permeabilised in 2% paraformaldehyde and 0.1% Triton X-100 for 30 min at 4°C. Cells were then incubated with primary antibodies overnight at 4°C, followed by the secondary antibodies (Alexa Fluor 488-labelled anti-mouse IgG; Alexa Fluor 568-labelled anti-rabbit IgG, Invitrogen, CA, USA) and the DNA stain 4′, 6-diamidino-2-phenylindole dihydrochloride (DAPI, Invitrogen) for 1 h at room-temperature. The stained cells were examined using a BZ-9000 fluorescence microscope (Keyence, Osaka, Japan).

Flow Cytometry. pTRE3G-ZsGreen1 vector, provided with the Tet-On 3G System kit (Clontech, CA, USA), was used to express ZsGreen simultaneously with the WT-, GSM-, or NSM-tuberin utilising the internal ribosome entry site (IRES) sequence according to the manufacturer's instructions. Single-cell suspensions were obtained by filtrating through a 40-μm filter. Cell sorting was performed on single-cell suspensions using an Epics Altra flow cytometer (Beckman Coulter, CA, USA). A sample flow was irradiated with a sapphire laser (wavelength: 488 nm), and the intensities of the forward scatter and fluorescence around 525 nm were collected (20,000 particles/sample). ZsGreen-positive cells were sorted at less than 700 events/s.

Animal studies and histological analyses. The animal experiments were performed in accordance with a protocol approved by Juntendo University, Tohoku University, and PhoenixBio Inc. Tissues from embryos were fixed in 10% buffered formalin, embedding in paraffin, sectioned, and routine histological examinations were performed after haematoxylin and eosin staining. For immunostaining, tissue sections were deparaffinised, preheated in 10 mM sodium citrate buffer (pH 6.0) in a microwave oven, and pretreated with 3% H_2O_2 solution for 10 min. Blocking was performed using 5% normal goat serum in wash buffer (1% BSA, Tris-buffered saline, 0.1% Tween 20, 0.07% NaN_3). Then, sections were incubated with the primary antibody (1/200 dilution in wash buffer) overnight at 4°C. Antibody binding was detected using the Envision system (DAKO, Glostrup, Denmark) using 3,3′-diaminobenzidine tetrahydrochloride (DAB; Dojindo, Kumamoto, Japan) as the substrate for peroxidase, followed by counterstaining with haematoxylin.

Phospho-Receptor Tyrosine Kinase (RTK) Array analysis. Phospho-RTK array analysis was performed using the Proteome Profiler Array Kit (R&D Systems, Minneapolis, MN, USA) according to the manufacturer's instructions. Briefly, transiently transfected HEK293 cells were lysed in the provided lysis buffer, incubated with the provided membrane, and RTKs were captured by antibodies spotted on a membrane. Then, levels of Phospho-RTK were assessed using a horseradish peroxidase-conjugated phospho-tyrosine antibody followed by chemiluminescence detection. This analysis allows simultaneous detection of relative tyrosine phosphorylation status of 44 different RTKs, which are listed in Supplementary Note S1.

Reverse Phase Protein Array (RPPA) analysis. RPPA analysis was performed by the Carna Biosciences assay service (Kobe, Japan) as previously described[44]. Briefly, transiently transfected HEK293 cells were homogenised and prepared with RIPA buffer (Thermo Scientific, IL, USA) supplemented with phosphatase (Thermo Scientific) and protease inhibitor cocktails (Sigma). Serially diluted cell lysates (1 : 1, 1 : 2, 1 : 4, and 1 : 8) were spotted onto glass slides with an array in eight replicates. Signals from slides stained with anti-phospho antibodies were analysed with the SuperCurve algorithm[45] to obtain a single value of relative concentration for each lysate. The relative concentration values are represented as a heat map. The 180 targets of the anti-phospho antibodies utilised in this study are also shown in Supplementary Note S2.

1. Gomez, M. R., Sampson, J. R. & Whittemore, V. H. *Tuberous Sclerosis Complex.* (Oxford University Press, 1999).

2. van Slegtenhorst, M. *et al.* Identification of the tuberous sclerosis gene TSC1 on chromosome 9q34. *Science* **277**, 805–808 (1997).
3. European Chromosome 16 Tuberous Sclerosis Consortium. Identification and characterization of the tuberous sclerosis gene on chromosome 16. *Cell* **75**, 1305–1315 (1993).
4. Manning, B. D. & Cantley, L. C. Rheb fills a GAP between TSC and TOR. *Trends Biochem. Sci.* **28**, 573–576 (2003).
5. Li, Y., Corradetti, M. N., Inoki, K. & Guan, K. L. TSC2: filling the GAP in the mTOR signaling pathway. *Trends Biochem. Sci.* **29**, 32–38 (2004).
6. Martin, D. E. & Hall, M. N. The expanding TOR signaling network. *Curr. Opin. Cell Biol.* **17**, 158–166 (2005).
7. Ma, X. M. & Blenis, J. Molecular mechanisms of mTOR-mediated translational control. *Nat. Rev. Mol. Cell Biol.* **10**, 307–318 (2009).
8. Niida, Y. *et al.* Analysis of both TSC1 and TSC2 for germline mutations in 126 unrelated patients with tuberous sclerosis. *Hum. Mutat.* **14**, 412–422 (1999).
9. Jones, A. C. *et al.* Comprehensive mutation analysis of TSC1 and TSC2-and phenotypic correlations in 150 families with tuberous sclerosis. *Am. J. Hum. Genet.* **64**, 1305–1315 (1999).
10. Dabora, S. L. *et al.* Mutational analysis in a cohort of 224 tuberous sclerosis patients indicates increased severity of TSC2, compared with TSC1, disease in multiple organs. *Am. J. Hum. Genet.* **68**, 64–80 (2001).
11. Maheshwar, M. M. *et al.* The GAP-related domain of tuberin, the product of the TSC2 gene, is a target for missense mutations in tuberous sclerosis. *Hum. Mol. Genet.* **6**, 1991–1996 (1997).
12. Jansen, A. C. *et al.* Unusually mild tuberous sclerosis phenotype is associated with TSC2 R905Q mutation. *Ann. Neurol.* **60**, 528–539 (2006).
13. Wentink, M. *et al.* Functional characterization of the TSC2 c.3598C>T (p.R1200W) missense mutation that co-segregates with tuberous sclerosis complex in mildly affected kindreds. *Clin. Genet.* **81**, 453–461 (2012).
14. Nellist, M. *et al.* Distinct effects of single amino-acid changes to tuberin on the function of the tuberin-hamartin complex. *Eur. J. Hum. Genet.* **13**, 59–68 (2005).
15. Mayer, K., Goedbloed, M., van Zijl, K., Nellist, M. & Rott, H. D. Characterisation of a novel TSC2 missense mutation in the GAP related domain associated with minimal clinical manifestations of tuberous sclerosis. *J. Med. Genet.* **41**, e64 (2004).
16. Nellist, M. *et al.* TSC2 missense mutations inhibit tuberin phosphorylation and prevent formation of the tuberin-hamartin complex. *Hum. Mol. Genet.* **10**, 2889–2898 (2001).
17. Shah, O. J. & Hunter, T. Critical role of T-loop and H-motif phosphorylation in the regulation of S6 kinase 1 by the tuberous sclerosis complex. *J. Biol. Chem.* **279**, 20816–20823 (2004).
18. Eker, R. & Mossige, J. A dominant gene for renal adenomas in the rat. *Nature* **189**, 858–859 (1961).
19. Yeung, R. S. *et al.* Predisposition to renal carcinoma in the Eker rat is determined by germ-line mutation of the tuberous sclerosis 2 (TSC2) gene. *Proc. Natl. Acad. Sci. U. S. A.* **91**, 11413–11416 (1994).
20. Hino, O. *et al.* The predisposing gene of the Eker rat inherited cancer syndrome is tightly linked to the tuberous sclerosis (TSC2) gene. *Biochem. Biophys. Res. Commun.* **203**, 1302–1308 (1994).
21. Kobayashi, T., Hirayama, Y., Kobayashi, E., Kubo, Y. & Hino, O. A germline insertion in the tuberous sclerosis (Tsc2) gene gives rise to the Eker rat model of dominantly inherited cancer. *Nat. Genet.* **9**, 70–74 (1995).
22. Kobayashi, T. *et al.* Transgenic rescue from embryonic lethality and renal carcinogenesis in the Eker rat model by introduction of a wild-type Tsc2 gene. *Proc. Natl. Acad. Sci. U. S. A.* **94**, 3990–3993 (1997).
23. Shiono, M. *et al.* The G1556S-type tuberin variant suppresses tumor formation in tuberous sclerosis 2 mutant (Eker) rats despite its deficiency in mTOR inhibition. *Oncogene* **27**, 6690–6697 (2008).
24. Momose, S. *et al.* Identification of the coding sequences responsible for Tsc2-mediated tumor suppression using a transgenic rat system. *Hum. Mol. Genet.* **11**, 2997–3006 (2002).
25. Hino, O. *et al.* Spontaneous and radiation-induced renal tumors in the Eker rat model of dominantly inherited cancer. *Proc. Natl. Acad. Sci. U. S. A.* **90**, 327–331 (1993).
26. Rennebeck, G. *et al.* Loss of function of the tuberous sclerosis 2 tumor suppressor gene results in embryonic lethality characterized by disrupted neuroepithelial growth and development. *Proc. Natl. Acad. Sci. U. S. A.* **95**, 15629–15634 (1998).
27. Kobayashi, T. *et al.* Renal carcinogenesis, hepatic hemangiomatosis, and embryonic lethality caused by a germ-line Tsc2 mutation in mice. *Cancer Res.* **59**, 1206–1211 (1999).
28. Kobayashi, T. *et al.* A germ-line Tsc1 mutation causes tumor development and embryonic lethality that are similar, but not identical to, those caused by Tsc2 mutation in mice. *Proc. Natl. Acad. Sci. U. S. A.* **98**, 8762–8767 (2001).
29. Luan, F. L., Hojo, M., Maluccio, M., Yamaji, K. & Suthanthiran, M. Rapamycin blocks tumor progression: unlinking immunosuppression from antitumor efficacy. *Transplantation* **73**, 1565–1572 (2002).
30. Meric-Bernstam, F. & Gonzalez-Angulo, A. M. Targeting the mTOR signaling network for cancer therapy. *J. Clin. Oncol.* **27**, 2278–2287 (2009).
31. Guba, M. *et al.* Rapamycin inhibits primary and metastatic tumor growth by antiangiogenesis: involvement of vascular endothelial growth factor. *Nat. Med.* **8**, 128–135 (2002).
32. Hudes, G. *et al.* Temsirolimus, interferon alfa, or both for advanced renal-cell carcinoma. *N. Engl. J. Med.* **356**, 2271–2281 (2007).
33. Atkins, M. B. *et al.* Randomized phase II study of multiple dose levels of CCI-779, a novel mammalian target of rapamycin kinase inhibitor, in patients with advanced refractory renal cell carcinoma. *J. Clin. Oncol.* **22**, 909–918 (2004).
34. Motzer, R. J. *et al.* Efficacy of everolimus in advanced renal cell carcinoma: a double-blind, randomised, placebo-controlled phase III trial. *Lancet* **372**, 449–456 (2008).
35. Yao, J. C. *et al.* Everolimus for advanced pancreatic neuroendocrine tumors. *N. Engl. J. Med.* **364**, 514–523 (2011).
36. Dutcher, J. P. Recent developments in the treatment of renal cell carcinoma. *Ther. Adv. Urol.* **5**, 338–353 (2013).
37. Abraham, R. T. Mammalian target of rapamycin: immunosuppressive drugs uncover a novel pathway of cytokine receptor signaling. *Curr. Opin. Immunol.* **10**, 330–336 (1998).
38. Kahan, B. D., Julian, B. A., Pescovitz, M. D., Vanrenterghem, Y. & Neylan, J. Sirolimus reduces the incidence of acute rejection episodes despite lower cyclosporine doses in caucasian recipients of mismatched primary renal allografts: a phase II trial. Rapamune Study Group. *Transplantation* **68**, 1526–1532 (1999).
39. Sehgal, S. N. Sirolimus: its discovery, biological properties, and mechanism of action. *Transplant. Proc.* **35**, 7S–14S (2003).
40. Krueger, D. A. *et al.* Everolimus for subependymal giant-cell astrocytomas in tuberous sclerosis. *N. Engl. J. Med.* **363**, 1801–1811 (2010).
41. Strizheva, G. D. *et al.* The spectrum of mutations in TSC1 and TSC2 in women with tuberous sclerosis and lymphangiomyomatosis. *Am. J. Respir. Crit. Care Med.* **163**, 253–258 (2001).
42. Khare, L. *et al.* A novel missense mutation in the GTPase activating protein homology region of TSC2 in two large families with tuberous sclerosis complex. *J. Med. Genet.* **38**, 347–349 (2001).
43. Hochi, S., Ninomiya, T., Waga-Homma, M., Sagara, J. & Yuki, A. Secretion of bovine alpha-lactalbumin into the milk of transgenic rats. *Mol. Reprod. Dev.* **33**, 160–164 (1992).
44. Masuda, M. *et al.* Alternative mTOR signal activation in sorafenib-resistant hepatocellular carcinoma cells revealed by array-based pathway profiling. *Mol. Cell. Proteomics,* [Epub ahead of print] (2014).
45. Tabus, I. *et al.* Nonlinear Modeling of Protein Expressions in Protein Arrays. *IEEE Transaction on Signal Processing* **54**, 2394–2407 (2006).

Acknowledgments

This research was supported by a Grant-in-aid for Cancer Research from the Ministry of Education, Culture, Sports, Science, and Technology of Japan. We thank M. Abe and Y. Sugiura for their technical assistance.

Author contributions

M.S. and T.K. designed the study; M.S., T.K. and R.T. performed experiments and analysed data; M.S. and T.K. wrote the manuscript; M.U., C.I. and O.H. gave technical support and conceptual advice.

Additional information

Supplementary information accompanies this paper at http://www.nature.com/scientificreports

Competing financial interests: The authors declare no competing financial interests.

How to cite this article: Shiono, M. *et al.* Transgenic expression of the N525S-tuberin variant in *Tsc2* mutant (Eker) rats causes dominant embryonic lethality. *Sci. Rep.* **4**, 5927; DOI:10.1038/srep05927 (2014).

SCIENTIFIC REPORTS

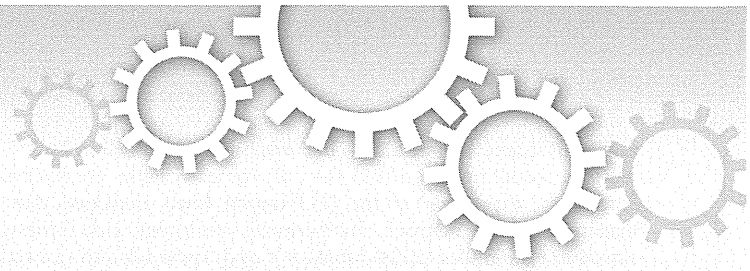

OPEN

SUBJECT AREAS:
MOLECULAR NEUROSCIENCE
DISEASES

Received
6 February 2014

Accepted
15 May 2014

Published
3 June 2014

Correspondence and requests for materials should be addressed to K.Y. (yamagata-kn@igakuken.or.jp)

* These authors contributed equally to this work.

Activation of Rheb, but not of mTORC1, impairs spine synapse morphogenesis in tuberous sclerosis complex

Shin Yasuda[1]*, Hiroko Sugiura[1]*, Shutaro Katsurabayashi[2], Tadayuki Shimada[1], Hidekazu Tanaka[3], Kotaro Takasaki[2], Katsunori Iwasaki[2], Toshiyuki Kobayashi[4], Okio Hino[4] & Kanato Yamagata[1]

[1]Neural Plasticity Project, Tokyo Metropolitan Institute of Medical Science, Tokyo, Japan, [2]Department of Neuropharmacology, Faculty of Pharmaceutical Sciences, Fukuoka University, Fukuoka, Japan, [3]Department of Biomedical Sciences, College of Life Sciences, Ritsumeikan University, Shiga, Japan, [4]Department of Pathology and Oncology, Juntendo University, School of Medicine, Tokyo, Japan.

Mutations in the *Tsc1* or *Tsc2* genes cause tuberous sclerosis complex (TSC). Tsc1 and Tsc2 proteins form a complex that inhibits mammalian target of rapamycin complex 1 (mTORC1) signalling through Rheb-GTPase. We found that $Tsc2^{+/-}$ neurons showed impaired spine synapse formation, which was resistant to an mTORC1 inhibitor. Knockdown of mTOR also failed to restore these abnormalities, suggesting mTORC may not participate in impaired spinogenesis in $Tsc2^{+/-}$ neurons. To address whether Rheb activation impairs spine synapse formation, we expressed active and inactive forms of Rheb in WT and $Tsc2^{+/-}$ neurons, respectively. Expression of active Rheb abolished dendritic spine formation in WT neurons, whereas inactive Rheb restored spine synapse formation in $Tsc2^{+/-}$ neurons. Moreover, inactivation of Rheb with farnesyl transferase inhibitors recovered spine synapse morphogenesis in $Tsc2^{+/-}$ neurons. In conclusion, dendritic spine abnormalities in TSC neurons may be caused through activation of Rheb, but not through of mTORC1.

In the mammalian brain, dendritic spines make most excitatory synapses. During development, synapse formation and elimination are accompanied by changes in dendritic spine number and morphology, allowing the establishment and remodelling of neuronal circuits. Structural plasticity of dendritic spines is tightly correlated with synaptic function and plasticity; even subtle changes in dendritic spines may have marked effects on synaptic plasticity. In particular, a large number of brain disorders, including developmental disorders are accompanied by disease-related changes in dendritic spine density and/or morphology.

Tuberous sclerosis complex (TSC) is a systemic genetic disease that causes the growth of hamartomas in the brain and other organs[1]. The neurological symptoms of TSC include mental retardation, intractable epilepsy, and autism[1]. TSC results from inactivating mutations in either *Tsc1*[2] or *Tsc2*[3], which encode hamartin and tuberin, respectively. Hamartin and tuberin form a complex that exhibits guanosine triphosphatase (GTPase)-activating protein (GAP) activity toward Rheb, a Ras-like small G-protein[4–6]. Inactivating mutations in *Tsc1* or *Tsc2* result in the accumulation of the GTP-bound form of Rheb, which activates mammalian target of rapamycin complex 1 (mTORC1)[7]. The mTOR is a serine/threonine protein kinase that stimulates translation initiation processes involving both eIF4E/4E-binding protein (4EBP) and p70S6 kinase/ribosomal S6 protein.

Mouse models that harbor a mutation in the *Tsc1* or *Tsc2* genes have been extensively investigated to clarify the mechanisms of the pathogenesis of TSC. Several lines of evidence suggest that these TSC model mice exhibit impairments in dendritic spine formation[8], long-term depression and cognitive behaviors[9], suggesting that activation of mTORC1 in TSC neurons may cause memory disturbance probably through dendritic spine abnormalities. However, the mTOR signaling has been demonstrated to be activated during learning and is required for spatial memory formation[10]. This controversy may suggest that another mechanism other than the mTOR signaling could be involved in memory impairment in TSC.

In the present study, we first confirmed that dendritic spine formation was abrogated and also excitatory spine synapses were drastically reduced in cultured rat $Tsc2^{+/-}$ neurons. This observation was consistent with the finding that filopodia-like protrusions were increased in $Tsc2^{+/-}$ rat brain. We treated cultured $Tsc2^{+/-}$ neurons with rapamycin, a specific mTORC1 inhibitor; however, it did not restore spine morphology but rather elongated dendritic protrusions. Knockdown of mTOR did not restore spine synapse formation either, suggesting that the mTORC pathway may not participate in spine synapse morphogenesis. We therefore focused on Rheb upstream

of mTORC1, and expressed the GDP-bound form of Rheb in $Tsc2^{+/-}$ neurons, resulting in restoration of spine synapse formation. Conversely, expression of the GTP-bound Rheb abolished spine formation in WT neurons. Furthermore, treatment with farnesyl transferase inhibitors (FTIs) lonafarnib and tipifarnib also rescued spine synapse formation in $Tsc2^{+/-}$ neurons. Taken together, these results suggest that spine synapse deformity in TSC neurons may be dependent on the state of Rheb, but not on mTORC activation.

Results

$Tsc2^{+/-}$ neurons show impaired spine synapse formation. In this study, we used spontaneous *Tsc2*-mutated Eker rats as animal models of TSC[11]. We first compared dendritic spine morphology of cultured hippocampal neurons of wild type (WT) and heterozygous Eker ($Tsc2^{+/-}$) rats. At 21 days in vitro (DIV), the dendritic spines of WT neurons displayed mushroom-type spines (Fig. 1a)(top), whereas the dendrites of $Tsc2^{+/-}$ neurons possessed long, thin filopodia (Fig. 1a)(bottom). Quantification showed the *Tsc2* mutation reduced the width of dendritic protrusions (Fig. 1a, b) and increased their length (Fig. 1a, c). To assess the influence of *Tsc2* haploinsufficiency on spine synapse formation, we immunolabelled neurons with vesicular glutamate transporter 1 (vGlut1), a presynaptic excitatory marker. In $Tsc2^{+/-}$ neurons, dendritic vGlut1 puncta were rarely located on protrusions but preferentially localized to dendritic shafts (Fig. 1a, d, e), indicating that $Tsc2^{+/-}$ growth cones form synapses with dendritic shafts.

Next, to confirm whether dendritic protrusions of *in vivo* $Tsc2^{+/-}$neurons exhibit similar morphological changes to those in cultured $Tsc2^{+/-}$neurons, we labeled hippocampal CA1 neurons in WT and $Tsc2^{+/-}$fixed brain tissues with biolistic-DiI (Fig. 1f). We observed similar morphological changes in spine width and length in $Tsc2^{+/-}$ neurons *in vivo* (Fig. 1g, h) to those observed in cultured $Tsc2^{+/-}$ neurons.

The mTORC1 inhibitor rapamycin does not restore spine synapse morphogenesis in $Tsc2^{+/-}$ neurons. To address whether the effects of *Tsc2* haploinsufficiency on neuronal morphology are mediated by elevated mTORC1 activity, we examined the ability of rapamycin to reverse defects in neuronal morphology. WT and $Tsc2^{+/-}$ hippocampal neurons were treated with rapamycin and maintained for 6 days. Application of rapamycin to $Tsc2^{+/-}$ neurons completely abolished the phosphorylation of S6 ribosomal protein, which is a substrate of the mTORC1 downstream target S6 kinase[12] (Fig. 2a, Supplementary Fig. S4a, b). Although rapamycin did not affect spine morphology in WT neurons (Fig. 2b, c, d), it rather induced the growth of long, thin protrusions in $Tsc2^{+/-}$ neurons (Fig. 2b, c, d) without restoration of spine synapse formation (Fig. 2b, e, f). To test whether mTORC2 participates in spine synapse formation, we next knocked down mTOR in WT and $Tsc2^{+/-}$ neurons by genetic silencing with siRNA (Supplementary Fig. S1). However, mTOR siRNA did not reverse spine synapse formation but rather elongated dendritic protrusions in $Tsc2^{+/-}$ neurons, like rapamycin treatment (Fig. 2g–k). The mTOR inhibition by either rapamycin or siRNA did not significantly change the number of spine synapses (Fig. 2e, f, j, k). Thus, neither mTORC1 nor mTORC2 may participate in the impaired spine synapse morphogenesis in TSC neurons.

Inactivation of Rheb recovers spine synapse formation in $Tsc2^{+/-}$ neurons. We therefore focused on Rheb, a GTPase located downstream of the Tsc1/2 complex and upstream of mTORC1, and examined whether Rheb activation is directly involved in spine synapse abnormalities in $Tsc2^{+/-}$ neurons. We first asked whether activation of Rheb in WT neurons causes morphological changes similar to those in $Tsc2^{+/-}$ neurons. To address this question, we expressed two kinds of Rheb mutants Gln64Val ($Rheb^{Q64V}$) and Asp60Ile ($Rheb^{D60I}$) in WT or $Tsc2^{+/-}$ neurons (Supplementary Fig. S2a, b). Gln64 mutant of Rheb displays a higher basal GTP level[5], whereas $Rheb^{D60I}$ mutation interferes selectively with GTP binding[13]. Expression of the $Rheb^{Q64V}$ completely abolished spine synapse formation in WT neurons, whose dendritic morphology was similar to that of $Tsc2^{+/-}$ neurons (Fig. 3a–e). In contrast, $Rheb^{Q64V}$ expression did not affect filopodia-like morphology of dendritic protrusions in $Tsc2^{+/-}$ neurons (Fig. 3a–c). Conversely, the expression of $Rheb^{D60I}$ restored spine synapse formation in $Tsc2^{+/-}$ neurons by increasing the ratio of spine synapses (Fig. 3f, i, j). $Rheb^{D60I}$ expression also rescued spine width in $Tsc2^{+/-}$ neurons to a similar extent to those in WT neurons (Fig. 3f, g). However, overexpression of $Rheb^{D60I}$ in WT neurons differentially modified their spine structure from those of $Tsc2^{+/-}$ neurons. $Rheb^{D60I}$ expression unexpectedly caused narrower and longer dendritic protrusions (Fig. 3f, g, h), and reduced the ratio of spine synapses in WT neurons (Fig. 3f, i, j). These results suggest that appropriate temporal activation of Rheb may be required for normal spine development in WT neurons. Thus, impaired spine synapse morphogenesis in $Tsc2^{+/-}$ neurons may be mediated by constitutively active state of Rheb and could be rescued by inactivation of Rheb.

FTI treatment restores spine synapse morphogenesis in $Tsc2^{+/-}$ neurons. To address whether pharmacological inactivation of Rheb recovers spine synapse formation in $Tsc2^{+/-}$ neurons, we utilized two kinds of FTIs, lonafarnib and tipifarnib. FTIs have been shown to reverse growth and actin filaments distribution in $Tsc1^{-/-}$ and $Tsc2^{-/-}$ cells in a rapamycin-sensitive and -insensitive manners[14]. Therefore, we treated $Tsc2^{+/-}$ neurons with lonafarnib or tipifarnib[15] for 3 days. These FTI treatments resulted in recuperation of F-actin accumulation in dendritic spines (Fig. 4a, b) and increases in spine synapse ratio (Fig. 4c–g) in $Tsc2^{+/-}$ neurons. On the other hand, either lonafarnib or tipifarnib treatment did not affect spine synapse formation in WT neurons (Fig. 4c, f, g). In conclusion, persistent activation of Rheb may abolish dendritic spine morphogenesis and that inactivation of Rheb with FTI may restore spine synapse formation in TSC neurons.

Finally, to reveal the functional differences in excitatory synaptic transmission between WT and $Tsc2^{+/-}$neurons, we measured evoked EPSC amplitude, mEPSC amplitude/frequency, readily releasable pool size and vesicular release probability from both cultured neurons. However, unexpectedly, synaptic transmission was sufficiently observed in cultured $Tsc2^{+/-}$ neurons without any significant difference in presynaptic or postsynaptic features between WT and $Tsc2^{+/-}$ neurons (Supplementary Fig. S3a–f). These results suggest that basal synaptic transmission may be preserved in $Tsc2^{+/-}$ neurons as WT neurons, irrespective of spine synapse abnormalities. Other electrophysiological properties, such as long-term depression, might be affected by impaired spine morphogenesis in $Tsc2^{+/-}$ neurons. Further studies are necessary for understanding the effects of morphological abnormalities of dendritic spines on the pathogenesis of TSC.

Discussion

In this paper, we have demonstrated activation of Rheb, not of mTORC1, is a main cause of dendritic spine synapse abnormality in $Tsc2^{+/-}$ neurons. We showed that active Rheb mutant abolished spine formation in WT neurons, whereas the inactive mutant of Rheb restored spine synapse morphogenesis in $Tsc2^{+/-}$ neurons. Furthermore, we demonstrated that FTI treatment, but not rapamycin treatment, rescued spine synapse morphology in $Tsc2^{+/-}$ neurons. These results, taken together, suggest that Rheb inhibition by FTI may be necessary for recovery of spine synapse formation in the TSC brain.

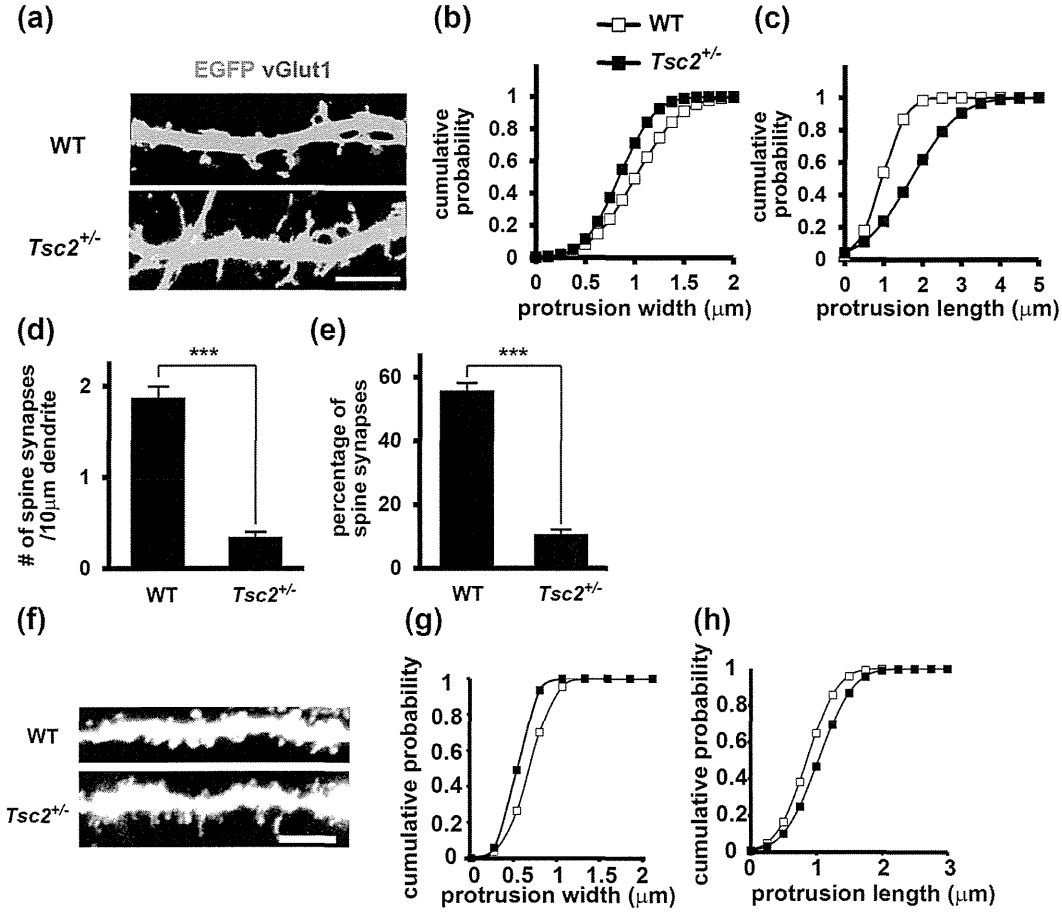

Figure 1 | *Tsc2* mutation suppresses dendritic spine synapse formation. (a) Images of dendrites from wild-type (top) and $Tsc2^{+/-}$ (bottom) pyramidal neurons in hippocampal culture. Neurons were transfected with *EGFP* and immunostained with anti-vGlut1 antibody. Scale bar, 10 μm. (b, c) Cumulative probability plots of protrusion width and length shown in (a). $Tsc2^{+/-}$ neurons showed a decrease in protrusion width (D = 0.2515, $P < 0.001$) and an increase in protrusion length (D = 0.4127, $P < 0.001$) compared with WT neurons (Kolmogorov-Smirnov test). (d) Densities of vGlut1-positive spine synapses in WT and $Tsc2^{+/-}$ neurons (***$P < 0.001$, unpaired, two-tailed *t*-test). (e) Percentage of spine synapses in WT and $Tsc2^{+/-}$ neurons (***$P < 0.001$, unpaired, two-tailed *t*-test). For each experiment (a–e), a total of 1,060/15/5 (WT) and 1,007/15/5 ($Tsc2^{+/-}$) protrusions/neurons/experiments were analysed, respectively. (f) Representative DiI-labelled dendrites of hippocampal CA1 neurons from WT and $Tsc2^{+/-}$ rats. Scale bar, 10 μm. (g, h) Cumulative probability plots of the protrusion width (g) and length (h) shown in (f). $Tsc2^{+/-}$ neurons showed a decrease in the protrusion width (D = 0.2950, $P < 0.001$) and an increase in the protrusion length (D = 0.2256, $P < 0.001$) compared with WT neurons (n = 1,001/12/6 (WT) and 1,034/12/6 ($Tsc2^{+/-}$) protrusions/neurons/experiments (Kolmogorov-Smirnov test).

Mouse models of TSC have demonstrated dendritic spine abnormalities that are resistant to rapamycin treatment[8,16]. For example, *Tsc1*-deficient mice develop several pathological features observed in human TSC patients. Rapamycin treatment improved neurofilament abnormalities, myelination and cell enlargement in *Tsc1*-ablated neurons, but it did not reverse dendritic spine morphology[17]. Additional studies have revealed that the application of rapamycin to *Tsc1*- or *Tsc2*-reduced neurons did not restore spine formation[8]. F-actin is the major cytoskeletal component in dendritic spines and has been thought to provide the structural basis for dendritic spines[18]. However, rapamycin has been shown to rather suppress F-actin reorganization in an mTOR-dependent manner[18–20]. Therefore, inhibition of F-actin reorganization by rapamycin might cause an elongation of existing filopodial protrusions, consistent with our results. Taken together, the impaired spine formation in TSC neurons may not be mediated by mTORC1.

Our results indicate that FTI treatment could restore morphological abnormalities in $Tsc2^{+/-}$ neurons. Farnesyl transferase (FT) recognizes the carboxyl-terminal CAAX box of small GTP-binding proteins and catalyses the transfer of lipid onto the cysteine residue. Following carboxymethylation of the farnesyl cysteine renders the carboxyl terminus more hydrophobic[21]. Membrane localization is essential for Rheb activity as for other small GTP-binding proteins[22]. To prevent Rheb farnesylation and membrane localization, FTIs have been used[14,23]. Unlike Ras, Rheb is not a substrate for geranylgeranyltransferases and can only undergo farnesylation[14]. Therefore, FTIs may suppress the Rheb activity mainly. On the other hand, another small GTP-binding protein RhoB has been shown to be an additional target of FTIs[24,25]. Because FTI treatment induces apoptosis in the endothelial cells of sprouting and developing blood vessels via inhibition of RhoB[25], pharmaceutical inactivation of RhoB could cause possible side effects as cardiovascular disorders where the angiogenesis would be desirable.

The finding that FTI was capable of restoring dendritic spine formation suggests that there are two different pathways downstream of Rheb in neurons, one signalling to neuronal growth and the other regulating neuronal morphology. The pathway affecting growth is likely to be mTORC1-dependent, whereas the pathway regulating neuronal morphology is rapamycin-insensitive. This mTORC1-dependent signalling is activated during learning and plays a crucial

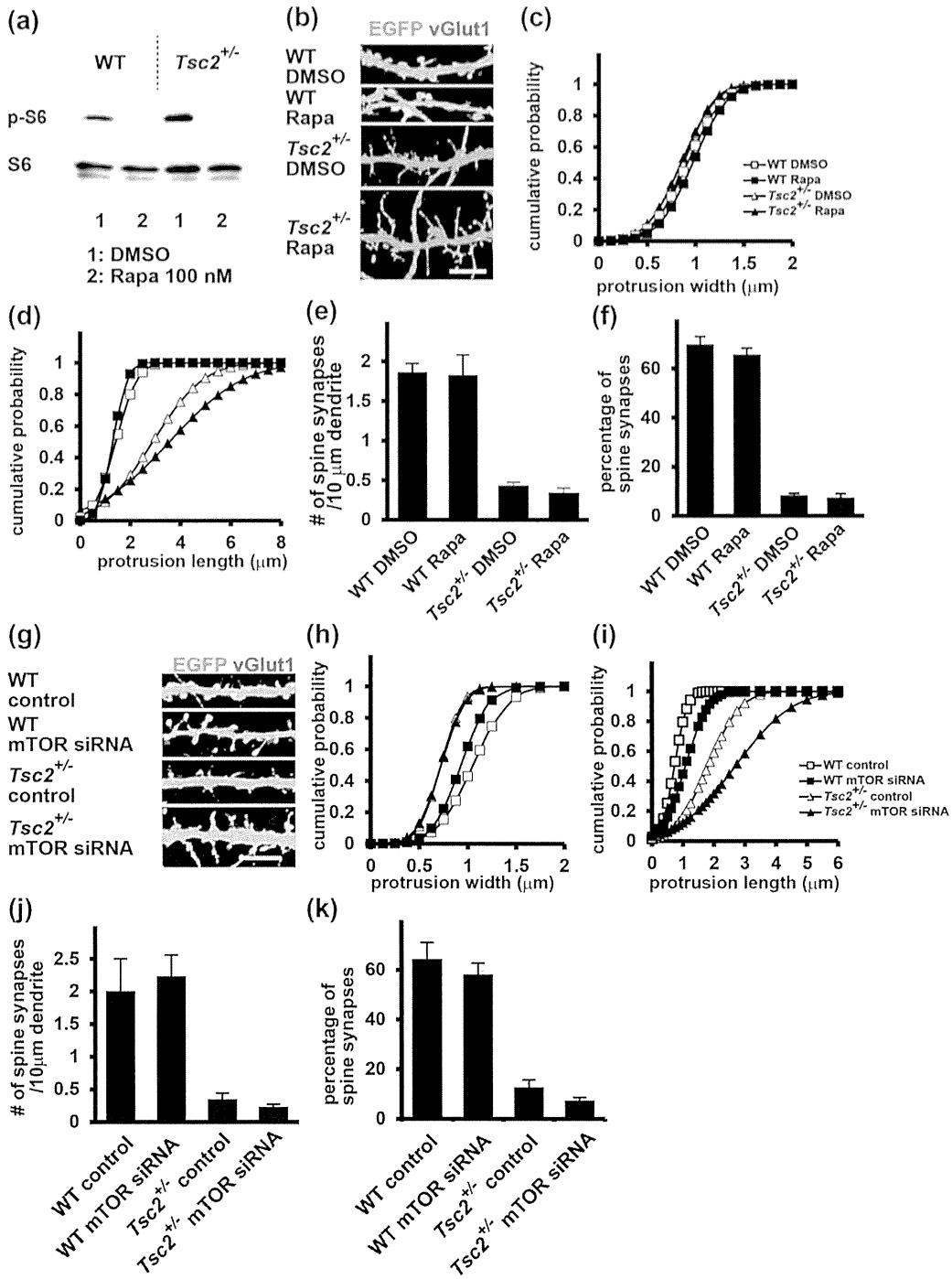

Figure 2 | Rapamycin fails to reverse spine synapse formation in *Tsc2*$^{+/-}$ neurons. (a) Rapamycin treatment completely abolished the phosphorylation of S6 in both WT and *Tsc2*$^{+/-}$ neurons. These blots are cropped, and full-length blots are presented in Supplementary Figure 1. (b) High-power images of the dendrites of DMSO- or 100 nM rapamycin-treated WT and *Tsc2*$^{+/-}$ neurons. Scale bar, 10 μm. (c, d) Cumulative probability plots of dendritic protrusion width (c) and length (d) in shown in (b). Note that rapamycin treatment increases dendritic protrusion lengths compared with DMSO treatment in *Tsc2*$^{+/-}$ neurons ($D = 0.1717$, $P < 0.001$, Kolmogorov-Smirnov test). (e) The densities of the vGlut1-positive spine synapses shown in (b). (f) The percentage of spine synapses in (b) (n = 400/7/3 (DMSO, WT), 400/7/3 (Rapa, WT), 1091/12/6 (DMSO, *Tsc2*$^{+/-}$) and 1020/12/6 (Rapa, *Tsc2*$^{+/-}$) protrusions/neurons/experiments). Note that rapamycin treatment did not significantly change the number of spine synapses. (g) Dendrites from control-, or mTOR siRNA-transfected WT and *Tsc2*$^{+/-}$ neurons. Scale bar, 10 μm. (h, i) Cumulative probability plots of protrusion width (h) and length (i) shown in (g). Note that mTOR siRNA expression causes increases in dendritic protrusion lengths in both WT and *Tsc2*$^{+/-}$ neurons, compared with scrambled siRNA ($D = 0.1684$, $P < 0.01$ (WT), $D = 0.3676$, $P < 0.001$ (*Tsc2*$^{+/-}$), Kolmogorov-Smirnov test). (j) The densities of the vGlut1-positive spine synapses shown in (g). (k) The percentage of spine synapses in (g) (n = 400/7/3 protrusions/neurons/experiments). Note that treatment with mTOR siRNA did not significantly change the number of spine synapses.

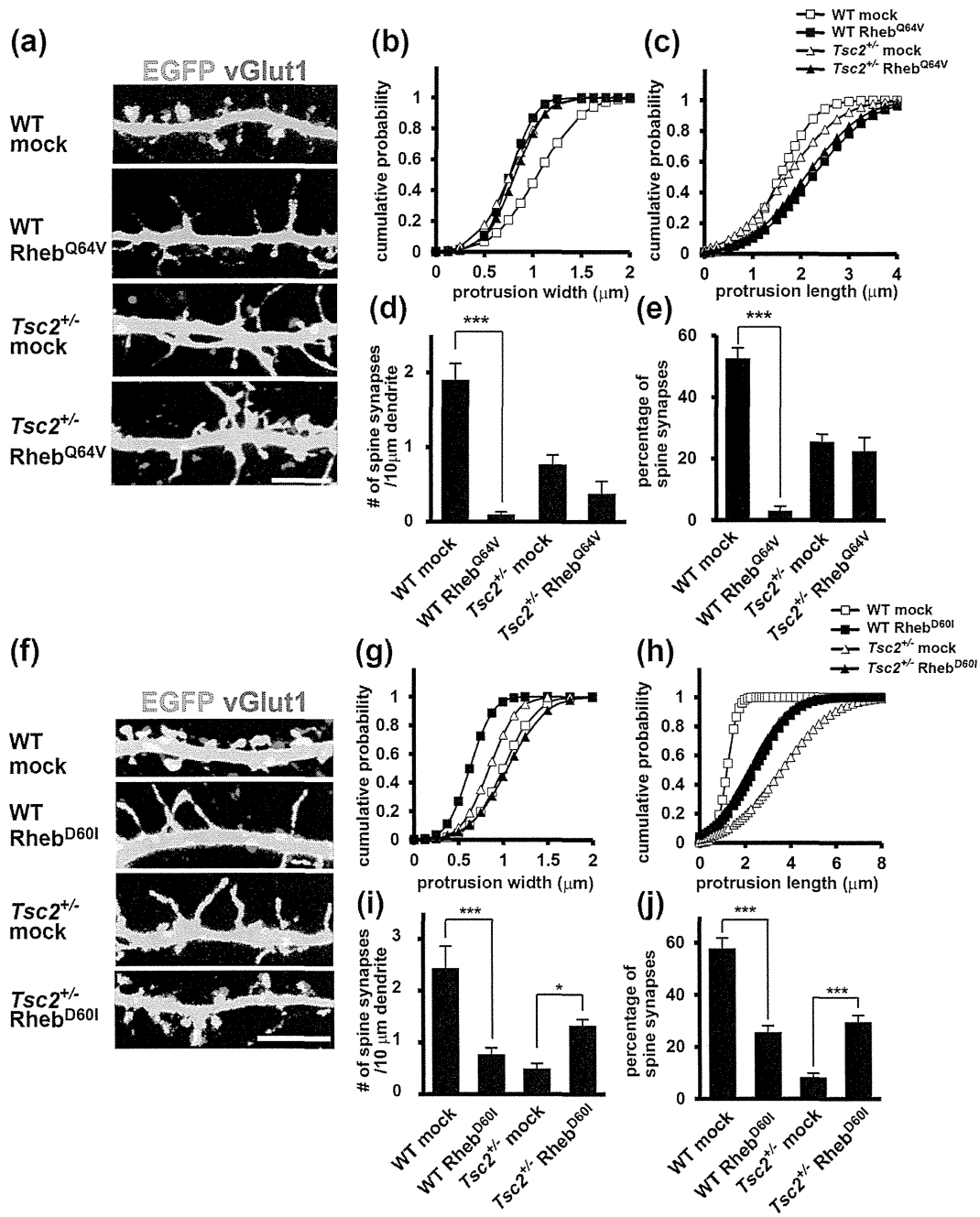

Figure 3 | Rheb regulates spine synapse formation. (a) Dendrites of EGFP- and mock- or FLAG-Rheb^{Q64V}-expressing hippocampal neurons prepared from WT and *Tsc2*$^{+/-}$ rats at DIV 19. Neurons were co-immunostained with anti-GFP and vGlut1 antibodies. Scale bar, 10 μm. (b, c) Cumulative probability distributions of protrusion width (b) and length (c) in (a). Rheb^{Q64V}-expressing WT neurons showed narrower (D = 0.2690, $P < 0.001$) and longer (D = 0.2391, $P < 0.001$) dendritic protrusions than mock transfectants (Kolmogorov-Smirnov test). (d) Quantification of the spine synapse densities shown in (a). (e) Percentage of spine synapses shown in (a). FLAG-Rheb^{Q64V}-expressing WT neurons showed few vGlut1-positive spines compared with mock-transfected neurons. The histograms show the mean values ± SEM (***$P < 0.001$, Two-Way ANOVA, post-hoc Tukey test). A total of 803/10/5 (WT, mock), 1,029/12/6 (WT, Rheb^{Q64V}), 501/6/3 (*Tsc2*$^{+/-}$, mock), 320/6/3 (*Tsc2*$^{+/-}$, Rheb^{Q64V}) protrusions/neurons/experiments, respectively, were analysed. (f) Dendrites of EGFP- and mock- or FLAG-Rheb^{D60I}-expressing hippocampal neurons prepared from WT and *Tsc2*$^{+/-}$ rats at DIV 19. Neurons were co-immunostained with anti-GFP and vGlut1 antibodies. Scale bar, 10 μm. (g, h) Cumulative probability plots of dendritic protrusion width (g) and length (h) in mock- or Rheb^{D60I}-expressing WT and *Tsc2*$^{+/-}$ neurons in (f). Note that Rheb^{D60I} increased dendritic protrusion width (D = 0.2903, $P < 0.001$) and decreased length (D = 0.4306, $P < 0.001$) in *Tsc2*$^{+/-}$ neurons, whereas Rheb^{D60I} decreased protrusion width (D = 0.638, $P < 0.001$) and increased length (D = 0.509, $P < 0.001$) in WT neurons, compared with mock transfectants (Kolmogorov-Smirnov test). (i) Quantitative analysis of the spine synapse density shown in (f). (j) The percentage of spine synapses in (f) (n = 300/6/3 (WT, mock), 300/6/3 (WT, Rheb^{D60I}), 988/12/6 (*Tsc2*$^{+/-}$, mock) and 1,044/12/6 (*Tsc2*$^{+/-}$, Rheb^{D60I}) protrusions/neurons/experiments, *$P < 0.05$, ***$P < 0.001$, Two-Way ANOVA, post-hoc Tukey test).

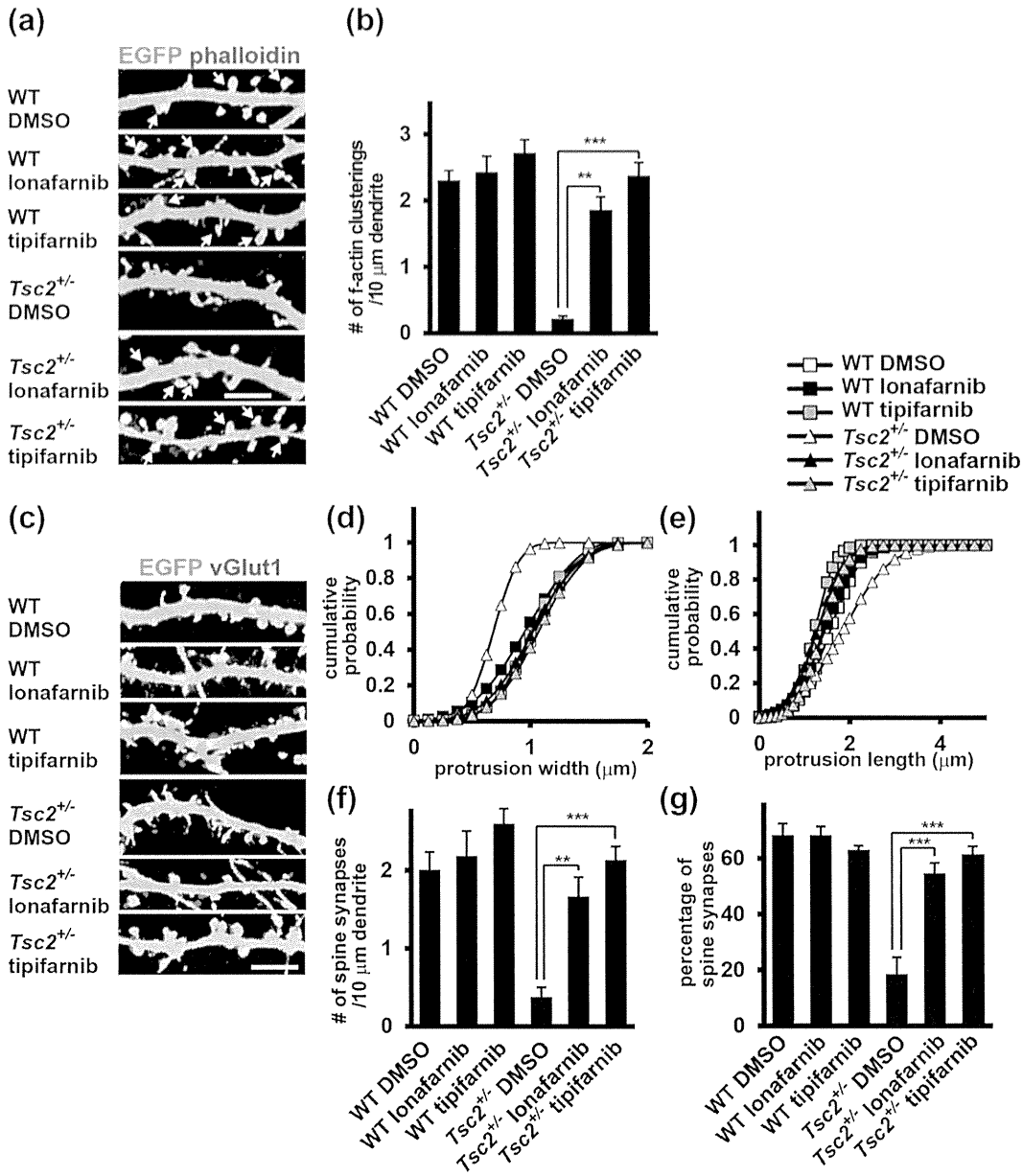

Figure 4 | FTI treatment restores spine synapse formation in $Tsc2^{+/-}$neurons. (a) Confocal images of cultured EGFP-expressing neurons from WT or $Tsc2^{+/-}$ hippocampi. Neurons were treated with DMSO, 2 μM lonafarnib or 2 μM tipifarnib for 3 days. F-actin was visualized with Alexa647-coupled phalloidin. Arrows denote positive puncta that are associated with dendritic spines. Scale bars, 10 μm. (b) Densities of the F-actin -positive spines shown in (a). (c) Immunodetection of vGlut1 (red)-positive presynaptic boutons in EGFP (green)-expressing WT and $Tsc2^{+/-}$ neurons treated with DMSO, lonafarnib or tipifarnib. (d, e) Cumulative probability distributions of protrusion width (d) and length (e) in (c). Note that lonafarnib or tipifarnib treatment increased dendritic protrusion width (D = 0.545, $P < 0.001$ (lonafarnib), D = 0.416, $P < 0.001$ (tipifarnib)) and decreased dendritic protrusion length (D = 0.367, $P < 0.001$ (lonafarnib), D = 0.242, $P < 0.001$ (tipifarnib)) compared with DMSO treatment in $Tsc2^{+/-}$ neurons (Kolmogorov-Smirnov test). (f) Quantification of vGlut1-positive spines in (c). (g) The percentage of spine synapses in (c) (n = 300/6/3 (WT, DMSO), 286/6/3 (WT, lonafarnib), 321/6/3 (WT, tipifarnib), 300/6/3($Tsc2^{+/-}$, DMSO), 376/6/3($Tsc2^{+/-}$, lonafarnib), 363/6/3 ($Tsc2^{+/-}$, tipifarnib) spines/neurons/experiments, $^{***}P < 0.001$, $^{**}P < 0.01$, Two-Way ANOVA, post hoc Tukey test).

role in the spatial learning[10]. By contrast, the TSC mice develop significant cognitive deficits[9]. This discrepancy might be explained by the notion that activation of the mTORC1-independent signalling may impair spine synapse formation in TSC and dominantly disturb memory acquisition or retention despite the mTORC1 activation.

What could be involved in the mTORC1-independent pathway to control neuronal morphology? We initially considered the possibility of the mTORC2 pathway; however, this seems unlikely, because mTOR knockdown fails to reverse spine synapse formation in $Tsc2^{+/-}$ neurons (Fig. 2g–k). Further experiments may provide important insights into how Rheb regulates neuronal morphology. As Rheb-mediated regulation of cytoskeleton has not been reported so far, we are currently searching Rheb-binding protein(s) in neurons. Clarification of this mechanism could extend our understanding of the prevailing role of Rheb in memory impairments in TSC patients.

Methods

Reagents. Rapamycin and FTIs (lonafarnib and tipifarnib) were purchased from LKT Laboratories and Toronto Research Chemicals, respectively. The used siRNAs are as follows: mTOR siRNA (CAGCAGCUGGUACAUGACAAGUACU and

AGUACUUGUCAUGUACCAGCUGCUG) and Stealth RNAi siRNA negative control kit. Oligonucleotides were synthesized and duplexed by Invitrogen.

Animals. The Eker (*Tsc2*$^{+/-}$) and wild-type (WT) genotypes were determined using PCR[26]. All animal experiments were approved by the Committee on the the Animal Care and Use Committees of the Tokyo Metropolitan Institute of Medical Science and Fukuoka University, and were performed according to their recommendation.

Primary culture and transfection. Primary culture and transfection of hippocampal neurons from *Tsc2*$^{+/-}$ and WT littermates (E20) have been previously described[27–29]. Cultured neurons were maintained in Neurobasal Medium supplemented with B27, gentamicin and GLUTAMAX. The neurons were transfected at DIV11–12 using Lipofectamine 2000 (Invitrogen) according to the manufacturer's instructions. Cultured hippocampal neurons were treated with 100 nM rapamycin for 6 days, 2 μM lonafarnib or 2 μM tipifarnib for 3 days. All experiments comparing WT and *Tsc2*$^{+/-}$ neurons were performed in parallel.

Spine and/or shaft synapse density analysis were performed as described previously[30]. Spines were defined as any protrusions from the dendritic shaft <8 μm in length. The number of vGlut1 puncta on spine and shaft synapses of the dendritic segment is determined by counting the number of vGlut1 puncta that are partially overlapping to the GFP-positive shaft or spines. Any vGlut1 puncta that are not touching the GFP-positive dendrite are not included.

Immunostaining. Rat cultured hippocampal neurons were fixed with 4% paraformaldehyde, blocked, permeabilized with BL solution (3% normal goat serum or 3% bovine serum albumin with 0.1% Triton X-100 in PBS), and incubated overnight at 4°C with one of the following primary antibodies: anti-GFP (chicken, Millipore), anti-phospho S6 (Ser235/236) (rabbit, CST), anti-phospho-Akt (Ser473) (rabbit, CST) or anti-vGlut1 (guinea pig, Millipore). The immunoreactivity was visualized using species-specific, fluorochrome-conjugated secondary antibodies. Neuronal F-actin was visualized by staining with Alexa Fluor 647 phalloidin (Invitrogen).

Image acquisition and quantification. Confocal images of neurons were obtained using a Zeiss 63× lens (NA 1.4) with sequential acquisition settings at the resolution of the confocal microscope (512 × 512 pixels). Each image was a composite constructed from a series of images captured throughout the *z* aspect of each cell. The parameters of each composite image were optimized for the particular lens and pinhole setting. Identical confocal microscope settings were maintained for all scans in each experiment. All morphometric analyses and quantifications were performed using MetaMorph image analysis software (Universal Imaging). For the spine morphology studies, individual dendritic protrusions were manually traced, and the maximum length and head width of each dendritic protrusion were measured and recorded in Microsoft Excel.

Diolistic labelling. Eight-week-old rats were deeply anesthetized with 0.1 mg/kg phenobarbital perfused transcardially with 0.1 M PB, followed by 50 ml of 2% PFA. The brains were dissected and post-fixed in the same fixative for 4 hr. Subsequently, sagittal brain sections were obtained using a vibratome and collected in PBS. Twenty-five milligrams of gold particles (Bio-Rad) were coated with 7.0 mg of the lipophilic dye DiI (Invitrogen) and injected into Tefzel tubing, which was subsequently cut into bullets. These particles were delivered diolistically at 80 psi using a Helios gene-gun system (Bio-Rad). The slices were fixed again with 4% PFA at 4°C for 1 hr and mounted on slides in VectaShield Mounting Medium (Vector Laboratories).

Western blot analysis. Western blot analyses of rat hippocampal neurons with anti-phospho S6 (Ser235/236) (rabbit, CST) antibody[31], anti-S6 (rabbit, CST) antibody[32] or HEK 293T cells with anti-mTOR antibody[33] were performed as described previously[29].

Autaptic culture. Astrocytes were obtained from cerebral cortices of newborn (P0) ICR mice (Kyudo). Cerebral cortices were removed from the brains, placed in cold Hank's Balanced Saline Solution (HBSS, Invitrogen) and dissociated with 0.05% trypsin-EDTA (Wako). The cells were plated in plating medium composed of Dulbecco's Modified Eagle Medium with GLUTAMAX and pyruvate (DMEM, Invitrogen) supplemented with 10% fetal bovine serum (FBS, Invitrogen) and 0.1% MITO+ Serum Extender (BD Biosciences). Two weeks later, astrocytes adhered to the bottom of the culture bottle were trypsinized and plated onto microdot-coated coverslips at a density of 6,000 cells/cm^2.

The autaptic cultures of E18–19 hippocampal neurons were generated in accordance with previous reports[34–36]. Briefly, CA1-CA3 hippocampi were isolated from embryo rats and enzymatically dissociated in papain (2 units/ml, Worthington) in DMEM. The dissociated hippocampal neurons were plated at a density of 1,500 cells/cm^2 onto the above astrocyte island plates. Before plating the dissociated neurons, the astrocyte-conditioned media was exchanged for Neurobasal-A medium (Invitrogen) supplemented with 2% B27 supplement (Invitrogen) and GLUTAMAX.

Electrophysiology. Synaptic responses from WT and *Tsc2*$^{+/-}$ autaptic neurons were recorded in the whole-cell configuration under the voltage-clamp mode at a holding potential (Vh) of −70 mV (MultiClamp 700B, Molecular Devices) and room temperature. The patch pipette resistance was 3–5 MΩ, and a series resistance was compensated by 70–90%. The AMPA receptor-mediated evoked glutamatergic synaptic transmission was recorded in response to an action potential elicited through a brief (2 ms) somatic depolarization pulse (to +0 mV) from the patch pipette. Spontaneous glutamatergic mEPSCs were recorded in the presence of 0.5 μM tetrodotoxin (TTX). The size of the readily releasable pool (RRP) of synaptic vesicles was estimated using a synaptic transient charge elicited through a 10 sec application of 0.5 M sucrose. The number of synaptic vesicles in the RRP was subsequently calculated by dividing the RRP charge by an individual average mEPSC charge. The vesicular release probability (P_{vr}) was calculated as the ratio of the charge of the evoked EPSC to the RRP charge successfully obtained from the same neuron. The synaptic responses were recorded at a sampling rate of 20 kHz and filtered at 10 kHz. The template for the mEPSC data analysis was set as a rise time constant of 0.5 ms, a decay time constant of 4 ms, a baseline of 5 ms, and a template length of 10 ms. The data were analysed off-line using Axograph X 1.2 software (AxoGraph Scientific). Recordings of synaptic responses were performed at DIV 7–9 for immature synapses and at DIV 19–22 for mature synapses.

The standard extracellular solution contained (in mM) NaCl 140, KCl 2.4, HEPES 10, glucose 10, $CaCl_2$ 2, and $MgCl_2$ 1, with pH 7.4 and an adjusted osmotic pressure of 315–320 mOsm. Patch pipettes were filled with an intracellular solution containing (in mM) K-gluconate 146.3, $MgCl_2$ 0.6, ATP-Na_2 4, GTP-Na_2 0.3, phosphocreatine 12, EGTA 1, and HEPES 17.8, as well as creatine phosphokinase 50 U/ml (pH 7.4). The extracellular solutions were applied using a fast-flow application system (Warner Instruments). All chemicals were purchased from Sigma-Aldrich unless otherwise specified.

Statistical analysis. The data were statistically analysed using Student's *t*-test, two-way ANOVA or the Kolmogorov-Smirnov test. Differences were considered significant when $p < 0.05$.

1. Crino, P. B., Nathanson, K. L. & Henske, E. P. The Tuberous Sclerosis Complex. *New Engl J Med* **355**, 1345–1356 (2006).
2. van Slegtenhorst, M. *et al.* Identification of the Tuberous Sclerosis Gene TSC1 on Chromosome 9q34. *Science* **277**, 805–808 (1997).
3. Kandt, R. S. *et al.* Linkage of an important gene locus for tuberous sclerosis to a chromosome 16 marker for polycystic kidney disease. *Nat Genet* **2**, 37–41 (1992).
4. Zhang, Y. *et al.* Rheb is a direct target of the tuberous sclerosis tumour suppressor proteins. *Nat Cell Biol* **5**, 578–581 (2003).
5. Inoki, K., Li, Y., Xu, T. & Guan, K.-L. Rheb GTPase is a direct target of TSC2 GAP activity and regulates mTOR signaling. *Genes Dev* **17**, 1829–1834 (2003).
6. Zou, J. *et al.* Rheb1 Is Required for mTORC1 and Myelination in Postnatal Brain Development. *Dev Cell* **20**, 97–108 (2011).
7. Manning, B. D. & Cantley, L. C. Rheb fills a GAP between TSC and TOR. *Trends Biochemi Sci* **28**, 573–576 (2003).
8. Tavazoie, S. F., Alvarez, V. A., Ridenour, D. A., Kwiatkowski, D. J. & Sabatini, B. L. Regulation of neuronal morphology and function by the tumor suppressors Tsc1 and Tsc2. *Nat Neurosci* **8**, 1727–1734 (2005).
9. Goorden, S. M. I., van Woerden, G. M., van der Weerd, L., Cheadle, J. P. & Elgersma, Y. Cognitive deficits in Tsc1+/− mice in the absence of cerebral lesions and seizures. *Ann Neurol* **62**, 648–655 (2007).
10. Qi, S., Mizuno, M., Yonezawa, K., Nawa, H. & Takei, N. Activation of mammalian target of rapamycin signaling in spatial learning. *Neurosci Res* **68**, 88–93 (2010).
11. Yeung, R. S. *et al.* Predisposition to renal carcinoma in the Eker rat is determined by germ-line mutation of the tuberous sclerosis 2 (TSC2) gene. *Proc Natl Acad Sci USA* **91**, 11413–11416 (1994).
12. Peterson, R. T. & Schreiber, S. L. Translation control: Connecting mitogens and the ribosome. *Curr Biol* **8**, R248–R250 (1998).
13. Tabancay, A. P. *et al.* Identification of Dominant Negative Mutants of Rheb GTPase and Their Use to Implicate the Involvement of Human Rheb in the Activation of p70S6K. *J Biol Chem* **278**, 39921–39930 (2003).
14. Gau, C.-L. *et al.* Farnesyltransferase inhibitors reverse altered growth and distribution of actin filaments in Tsc-deficient cells via inhibition of both rapamycin-sensitive and -insensitive pathways. *Mol Cancer Ther* **4**, 918–926 (2005).
15. Appels, N. M. G. M., Beijnen, J. H. & Schellens, J. H. M. Development of Farnesyl Transferase Inhibitors: A Review. *Oncologist* **10**, 565–578 (2005).
16. Meikle, L. *et al.* Response of a Neuronal Model of Tuberous Sclerosis to Mammalian Target of Rapamycin (mTOR) Inhibitors: Effects on mTORC1 and Akt Signaling Lead to Improved Survival and Function. *J Neurosci* **28**, 5422–5432 (2008).
17. Meikle, L. *et al.* A Mouse Model of Tuberous Sclerosis: Neuronal Loss of Tsc1 Causes Dysplastic and Ectopic Neurons, Reduced Myelination, Seizure Activity, and Limited Survival. *J Neurosci* **27**, 5546–5558 (2007).
18. Hotulainen, P. & Hoogenraad, C. C. Actin in dendritic spines: connecting dynamics to function. *J Cell Biol* **189**, 619–629 (2010).
19. Liu, L., Chen, L., Chung, J. & Huang, S. Rapamycin inhibits F-actin reorganization and phosphorylation of focal adhesion proteins. *Oncogene* **27**, 4998–5010 (2008).
20. Liu, L. *et al.* Rapamycin Inhibits Cytoskeleton Reorganization and Cell Motility by Suppressing RhoA Expression and Activity. *J Biol Chem* **285**, 38362–38373 (2010).
21. Gutierrez, L., Magee, A. I., Marshall, C. J. & Hancock, J. F. Post-translational processing of p21ras is two-step and involves carboxyl-methylation and carboxy-terminal proteolysis. *EMBO J* **8**, 1093–8 (1989).

22. Clark, G. J. *et al.* The Ras-related Protein Rheb Is Farnesylated and Antagonizes Ras Signaling and Transformation. *J Biol Chem* **272**, 10608–10615 (1997).
23. Basso, A. D. *et al.* The Farnesyl Transferase Inhibitor (FTI) SCH66336 (lonafarnib) Inhibits Rheb Farnesylation and mTOR Signaling: ROLE IN FTI ENHANCEMENT OF TAXANE AND TAMOXIFEN ANTI-TUMOR ACTIVITY. *J Biol Chem* **280**, 31101–31108 (2005).
24. Prendergast, G. C. Farnesyltransferase inhibitors: antineoplastic mechanism and clinical prospects. *Curr Opin Cell Biol* **12**, 166–173 (2000).
25. Adini, I., Rabinovitz, I., Sun, J. F., Prendergast, G. C. & Benjamin, L. E. RhoB controls Akt trafficking and stage-specific survival of endothelial cells during vascular development. *Genes Dev* **17**, 2721–2732 (2003).
26. Rennebeck, G. *et al.* Loss of function of the tuberous sclerosis 2 tumor suppressor gene results in embryonic lethality characterized by disrupted neuroepithelial growth and development. *Proc Natl Acad Sci USA* **95**, 15629–15634 (1998).
27. Irie, Y. *et al.* Molecular Cloning and Characterization of Amida, a Novel Protein Which Interacts with a Neuron-specific Immediate Early Gene Product Arc, Contains Novel Nuclear Localization Signals, and Causes Cell Death in Cultured Cells. *J Biol Chem* **275**, 2647–2653 (2000).
28. Sugiura, H. *et al.* Inhibitory Role of Endophilin 3 in Receptor-mediated Endocytosis. *J Biol Chem* **279**, 23343–23348 (2004).
29. Yasuda, S. *et al.* Activity-Induced Protocadherin Arcadlin Regulates Dendritic Spine Number by Triggering N-Cadherin Endocytosis via TAO2[beta] and p38 MAP Kinases. *Neuron* **56**, 456–471 (2007).
30. Aoto, J. *et al.* Postsynaptic EphrinB3 Promotes Shaft Glutamatergic Synapse Formation. *J Neurosci* **27**, 7508–7519 (2007).
31. Fonseca, B. D. *et al.* Pharmacological and Genetic Evaluation of Proposed Roles of Mitogen-activated Protein Kinase/Extracellular Signal-regulated Kinase Kinase (MEK), Extracellular Signal-regulated Kinase (ERK), and p90RSK in the Control of mTORC1 Protein Signaling by Phorbol Esters. *J Biol Chem* **286**, 27111–27122 (2011).
32. Possemato, R. *et al.* Functional genomics reveal that the serine synthesis pathway is essential in breast cancer. *Nature* **476**, 346–50 (2011).
33. Gao, D. *et al.* mTOR Drives Its Own Activation via SCFβTrCP-Dependent Degradation of the mTOR Inhibitor DEPTOR. *Mol Cell* **44**, 290–303 (2011).
34. Wojcik, S. M. *et al.* A Shared Vesicular Carrier Allows Synaptic Corelease of GABA and Glycine. *Neuron* **50**, 575–587 (2006).
35. Pyott, S. J. & Rosenmund, C. The effects of temperature on vesicular supply and release in autaptic cultures of rat and mouse hippocampal neurons. *J Physiol* **539**, 523–535 (2002).
36. Burgalossi, A. *et al.* Analysis of neurotransmitter release mechanisms by photolysis of caged Ca2+ in an autaptic neuron culture system. *Nat. Protocols* **7**, 1351–1365 (2012).

Acknowledgments

We are grateful to K. Kohyama and Y. Matsumoto for gene gun; T. Yamauchi for invaluable advice. This work was supported by JSPS KAKENHI Grant Number 24659093, 25293239, MEXT KAKENHI Grant Number 23110525, 25110737, and a grant from the Naito Foundation.

Author contributions

K.Y., S.Y. and H.S. designed research; S.Y., H.S., S.K., T.S., K.T., K.I., T.K., O.H. and K.Y. performed experiments; H.T. analysed data; and K.Y., S.Y. and H.S. wrote the manuscript. All authors reviewed the manuscript.

Additional information

Supplementary information accompanies this paper at http://www.nature.com/scientificreports

Competing financial interests: The authors declare no competing financial interests.

How to cite this article: Yasuda, S. *et al.* Activation of Rheb, but not of mTORC1, impairs spine synapse morphogenesis in tuberous sclerosis complex. *Sci. Rep.* **4**, 5155; DOI:10.1038/srep05155 (2014).

特集　WFSBP2013シンポジウム

5. 脳ペプタイドに関わる精神神経疾患の病態と治療的展望：ミトコンドリアの機能障害との関連

油井　邦雄*

抄録：本シンポジウムでは細胞死にかかわるペプタイドに関わるミトコンドリアの障害と精神神経疾患との関連，およびそれらの治療的展開を検討した。ミトコンドリアの膜上に存在するtranslocator protein（TSPO）はアポトーシスに関わり，そのリガンドは神経疾患の治療や診断に有益である。パーキンソン病はミトコンドリアの機能障害であり，PINK1酵素がParkinにswitch onしてリン酸を付加することで不良ミトコンドリアへ呼び寄せて発病に至る。正しくスイッチが入るようにして，不良ミトコンドリアを分解に導くことが治療につながる。MK-801はミトコンドリア機能保護作用があり，この統合失調症モデルはp70S6K-S6の回路におけるタンパクの形成の障害によるので，治療的展開に利用し得る。酸化ストレスによる脂質の過酸化過程はミトコンドリアの機能障害を惹起し，また，シグナル伝達機能を損ない，自閉症スペクトラムの病態要因になるので，antioxidantが治療的に有益である。

日本生物学的精神医学会誌 25（2）：85-89, 2014

Key words：mitochondorial dysfunction, translocator protein, MK-801, antioxidants

はじめに

ミトコンドリア（mitochondrion，複数形：mitochondria）は真核生物の細胞小器官であり，エネルギー産生，Ca^{2+}のシグナル伝達，ストレス応答やcell death（細胞死）など生体の機能に重要な役割を果たしている。ミトコンドリアの作用が低下すると，細胞の活動が低下して認知障害や運動障害が生じるし，パーキンソン病，アルツハイマー病，統合失調症，双極性障害，自閉症スペクトラム障害などの精神神経疾患の病因，病態になる。

ミトコンドリアの細胞外膜には18kDaタンパク（18 kDa locatorprotein）が存在し，このタンパクは免疫系における炎症反応，細胞死の惹起作用，ストレス適応反応を起こす（http://en.wikipedia.org/wiki/Translocator_protein）。他方，脳の保護作用[3]，軸索の再生[5]，脳内炎症反応の調整[5]，ミトコンドリア機能の調整[4, 5, 24]，ミトコンドリアのエネルギー産生[4]に関わり，脳におけるステロイドの産生[24]および抗不安作用を持ち[3]，末梢神経の損傷と軸索型ニューロパチーの治療効果を持ち，神経保護作用が期待できる[5]。

NMDA系の拮抗薬であるMK-801は無酸素・無グルコースによって惹起されるミトコンドリアの損傷を防止し得る[23]。また，ミトコンドリアが関わるドーパミン系神経の細胞の変性やアポトーシスを防止する[6]。

黒質線条体のミトコンドリア複合体の欠損はドーパミン系神経細胞の消滅をもたらし，パーキンソン病の病因になる[2]。パーキンソン病ではミトコンドリアタンパクの変異遺伝子（PINK1, parkinm, DJなど）の発見がミトコンドリア説の根拠になっている。しかし，ミトコンドリアはCa^{2+}のsignalingに関わっているので，この回路を対象とした治療，たとえばL-type Ca^{2+}チャンネル拮抗薬は発病初期の治療には有益であるとされる[19]。

自閉症スペクトラム障害（autism spectrum disorders, ASD）はニューロンネットワークの発達不全であり，その成因としてミトコンドリアの機能障害が指摘されている[11]。その背景要因として，免疫系の機能昂進[11]，Ca^{2+}イオンsignalingの異常[11]，酸化ストレス[11]，あるいは酸化ストレス反応性に放

The pathophysiological role and therapeutic potential of brain peptides in psychiatric disorders：traslocator protein and its related MK-801, and antioxidants

＊芦屋大大学院発達障害教育研究所（〒659-8511　兵庫県芦屋市六麓荘町13-22）Kunio Yui：Research Institute of Pervasive Developmental Disorders, Ashiya University. 13-22, rokurokuso-cho, Ashiya, Hyogo 659-8511, Japan

出される lymphoblastoid cell lines（リンパ芽球様細胞株）[16] の影響が挙げられている。ASD の病因として，酸化ストレスによるミトコンドリア機能の障害[15, 17]，脳の解剖学的発達の偏倚によるニューロンネットワークの機能不全[3] が ASD の中核症状である社会的相互性の障害の惹起につながると考えられている。酸化ストレスの影響については，数年前までは酸化ストレスの様相の異常[26]，酸化ストレスに対する脆弱性[12, 14] が病態として推察されたが，最近では酸化ストレスによる DAN 損傷と側頭部のミトコンドリアの機能障害[22]，あるいは酸化ストレスによるミトコンドリアの機能障害との関連[15] が唱えられ，ミトコンドリア機能が注目されている。油井ら[27] はアラキドン酸/DHA 比が 1/1 の製品による ASD の社会的相互性障害の改善に signaling の dawn-regulation と酸化ストレスが関与する可能性を指摘した。さらに，油井らは ω-6/ ω-3 の含有比がこの製品よりも高い新しい脂肪酸製品を用いて，行動異常と社会的相互性障害が著明に改善することをみて，さらに検索中である。また，奏功機序として signaling や antioxidant 機構，および DNA 損傷の様相をも併せて検索し，signaling と antioxidant のマーカーの有意な upregulation を見出しつつある。

このようにミトコンドリアの機能低下はパーキンソン病，ASD の病態要因になるが，MK-801, translocator protein がミトコンドリアの機能障害に対する拮抗作用を持つので，これらの治療的展開が期待できる。

1. Translocator protein as a therapeutic target for schizophrenia and major depression

(Rainer Rupprecht, Germany)

Translocator protein（TSPO）は中枢神経系のミトコンドリア膜にあるステロイド生成細胞に局在し，神経保護作用，軸索の再生，脳内炎症の調整を行っている。TSPO の発現は脳内炎症反応とそれに伴うグリオーシスを生成するので，このリガンドは画像診断の標識になる[18]。TSPO の過剰産出はパーキンソン氏病，アルツハイマー病などの神経疾患においてみられるので，これらの疾患の診断指標になる。すでに抗不安薬として使われている Etifoxine は TSPO を介するものであり，プロゲステロンの生成と代謝の増大を伴う[5]。Rupprecht らは TSPO のリガンドが神経の外傷的損傷モデルにおいて，耐性を生じることなしに抗炎症的な作用を生じることをみて[5]，TSPO のリガンドはミトコンドリア膜において，神経保護的なタンパクの生成を促進し，抗不安作用を示すことを推察した。Rupprecht らはこのことが各種精神神経疾患の治療の手段になり得ると提起した。

2. Pathophysiology of familial Parkinson'disease and potential biomarker for mitochondria stress

(Shigeto Sato, Nobutaka Hattori, Japan)

パーキンソン病の細胞内異常にはミトコンドリアの機能障害と酸化ストレスがかかわり，これらは環境と遺伝素因によってもたらされる。若年性遺伝性パーキンソン病の原因遺伝子として，PINK1 と Parkin が知られている[20]。Parkin は機能低下をきたしミトコンドリアを除去する働きをしていると考えられ，通常は働かない。不良ミトコンドリアが生じると，ミトコンドリア上にある酵素である PINK1 がそれを感知し，細胞質にある Parkin をミトコンドリア上に呼び寄せ，ミトコンドリアの分解が起こる[20]。この機序として，PINK1 が活性化して Parkin がリン酸化する過程が関与する[20]。したがって，Parkin に正しくスイッチが入るようにして，不良ミトコンドリアを分解してしまうことが本疾患の治療につながると期待される[20]（順天堂大学, News & Information, 2012 年 12 月 19 日）。Parkin のスイッチオンについて，Okatsu, Hattori ら[13] は健常なミトコンドリアでは PINK1 が迅速に分解されるが，膜電位が消失したミトコンドリアでは PINK1 が蓄積し，この PINK1 がミトコンドリア膜の電位の低下とともに Ser228 と Ser402 というリン酸化部位（phosphorylation sites）で自己リン酸化される。これらの 2 部位をアラニンに置換する変異を導入すると，PINK1 の自己リン酸化が起こらなくなり，膜電位が消失ないし低下したミトコンドリアへの Parkin の移行が阻害されるという[13]。これらを勘案すると，不良ミトコンドリアの蓄積をいち早く検出することが，パーキンソン病の早期診断法の鍵になるという（順天堂大学, News & Information, 2012 年 12 月 19 日）。